Supplementary Information (SI) for Chemical Science.
This journal is © The Royal Society of Chemistry 2026

Supporting Information

Efficient Pure-Red Multiple Resonance Emitter based on Donor Planarization Strategy

Linjie Li,[a] Yincai Xu,*[a] Dongyue Zhang,[b] Yupei Qu,[a] Yue Wang[a] and Chenglong Li*[a]

[a] L. Li, Y. Xu, Y. Qu, Prof. C. Li and Prof. Y. Wang

State Key Laboratory of Supramolecular Structure and Materials

College of Chemistry, Jilin University, Changchun 130012, P. R. China.

[b] D. Zhang

School of Chemistry and Pharmaceutical Engineering, Jilin Institute of Chemical Technology, Jilin 132022, P. R. China

*Corresponding Author(s): chenglongli@jlu.edu.cn (Chenglong Li); ycxu17@mails.jlu.edu.cn (Yincai Xu)

Table of Contents

1. Experimental Section

1.1. Materials and Methods

All reagents were purchased from *Energy Chemical Co.*, *Nanjing Kaimuco Technology Co., Ltd* and immediately used without further purification. The Schlenk technology was strictly performed under nitrogen condition in all reactions and the concrete synthetic procedures were showed below in detail. The final products were first purified by column chromatography, then temperature-gradient sublimation was utilized to further purify the target compounds under high vacuum to obtain highly pure samples. Thermo Fisher ITQ1100 GC/MS mass spectrometer was employed to measure the mass spectra. Flash EA 1112 spectrometer was used to perform the elemental analyses. ^{1}H NMR (500 MHz), ^{13}C NMR (125 MHz) spectra were recorded on Bruker AV 500 NMR (^{1}H NMR) and 600 NMR (^{13}C NMR) instrument at ambient temperature using deuterated solvents with tetramethylsilane (TMS) as the internal standard.

1.2. Synthesis

Synthesis of Cz-DF: 1,2-Difluoro-4-iodobenzene (25.00 g, 104.17 mmol), 3,6-*ditert*-butyl-9*H*-carbazole (9.70 g, 34.72 mmol), copper (Cu) (11.11 g, 173.60 mmol), 18-Crown-6 (9.18 g, 34.72 mmol) and potassium carbonate (K_2CO_3) (23.99 g, 173.60 mmol) were added with 250 mL 1,2-dichlorobenzene (*o*-DCB) under nitrogen atmosphere. Then the mixture was heated to 180 ℃ and stirred for 24 hours. After cooling to room temperature, the reaction mixture was extracted with dichloromethane and water, and the combined organic layer was condensed in vacuum, and the crude product was further purified by column chromatography with a mixture eluent of petroleum ether/dichloromethane (8:1) to afford a white solid (10.06 g, 25.69 mmol). Yield: 74%. ^{1}H NMR (500 MHz, DMSO-d_6) δ 8.18 (d, J = 1.9 Hz, 2H), 7.70 – 7.60 (m, 2H), 7.44 (dd, J = 8.6, 1.9 Hz, 3H), 7.28 (d, J = 8.6 Hz, 2H), 1.41 (s, 18H). ^{13}C NMR (151 MHz, DMSO-d_6) δ 150.8, 150.7, 149.2, 149.2, 149.1, 149.1, 147.6, 147.5, 142.8, 142.7, 138.4, 134.1, 134.1, 134.1, 134.1, 123.5, 123.5, 123.5, 122.9, 122.9, 118.7, 118.6, 116.6, 116.1, 115.9, 108.9, 39.9, 39.8, 39.6, 39.5, 39.4, 39.2, 39.1, 34.4, 34.4, 31.7. ESI-MS (M): m/z: 390.72 [M]+ (calcd: 391.51).

Synthesis of Cz-Br-DF: *N*-bromosuccinimide (NBS) (2.80 g, 15.75 mmol) was dissolved in *N*,*N*-dimethylformamide (DMF) (40 mL) and added dropwise to a solution of **Cz-DF** (5.87 g, 15.00 mmol) in DMF (60 mL) at 0 °C. Then the mixture was bubbled with nitrogen for 1 minute and stirred for 24 hours at room temperature. The reaction mixture was directly concentrated under reduced pressure and purified by column

chromatography with a mixture eluent of petroleum ether/dichloromethane (10:1) to afford a white solid (6.07 g, 12.90 mmol). Yield: 86%. ^{1}H NMR (500 MHz, DMSO-d_6) δ 8.21 (d, J = 1.7 Hz, 1H), 8.17 (d, J = 1.9 Hz, 1H), 7.57 – 7.46 (m, 3H), 7.42 (dd, J = 8.8, 1.9 Hz, 1H), 7.25 (dd, J = 8.9, 4.2 Hz, 1H), 6.94 (d, J = 8.6 Hz, 1H), 1.40 (d, J = 6.9 Hz, 18H). ^{13}C NMR (151 MHz, DMSO-d_6) δ 150.5, 150.4, 150.2, 150.1, 148.9, 148.8, 148.5, 148.5, 144.3, 143.4, 141.1, 135.5, 134.3, 134.3, 134.2, 134.2, 128.2, 126.9, 126.9, 126.8, 126.8, 126.2, 124.6, 122.0, 119.3, 117.7, 117.6, 116.7, 116.6, 116.5, 109.6, 108.9, 102.7, 40.0, 39.9, 39.7, 39.6, 39.5, 39.3, 39.2, 34.4, 34.4, 31.7, 31.6. ESI-MS (M): m/z: 471.00 [M]+ (calcd: 470.40).

Synthesis of Cz-Br-ICz-2: Cz-DF (6.07 g, 12.90 mmol), 11,12-dihydroindolo[*2*,*3*-*a*]carbazole (ICz) (13.56 g, 12.90 mmol) and cesium carbonate (Cs_2CO_3) (25.23 g, 77.40 mmol) were added with 160 mL DMF under nitrogen atmosphere. After stirring and refluxing for 72 h, the resulting solution was poured into ice water. The white powder solid was filtered out and dried in vacuum, and then further purified by column chromatography with a mixture eluent of dichloromethane/petroleum ether (1:7) to afford a white solid (2.30 g, 3.35 mmol). Yield: 26%. ^{1}H NMR (500 MHz, Methylene Chloride-d_2) δ 8.80 (dd, J = 7.6, 1.7 Hz, 2H), 8.43 (d, J = 8.6 Hz, 2H), 8.19 (d, J = 1.7 Hz, 2H), 7.93 (t, J = 2.1 Hz, 1H), 7.86 (d, J = 1.7 Hz, 1H), 7.70 (s, 1H), 7.66 – 7.59 (m, 4H), 7.55 – 7.50 (m, 1H), 7.40 (dd, J = 7.9, 2.0 Hz, 1H), 7.32 (d, J = 6.8 Hz, 1H), 7.21 (s, 1H), 7.08 (d, J = 1.8 Hz, 1H), 1.52 (s, 9H), 1.46 (s, 9H). ^{13}C NMR (151 MHz, CD_2Cl_2-d_6) δ 150.7, 149.5, 146.5, 145.8, 142.2, 139.4, 137.8, 134.9, 131.9, 131.2, 131.1, 130.3, 128.6, 127.2, 124.2, 122.3, 120.6, 120.3, 118.2, 117.3, 117.2, 116.3, 108.8, 105.3, 35.4, 35.2, 32.1, 32.0. ESI-MS (M): m/z: 687.18 [M]+ (calcd: 686.70).

Synthesis of RBN-ICz: A solution of *n*-butyllithium (*n*-BuLi) in pentane (2.36 mL, 2.50 M, 13.40 mmol) was slowly added to a solution of **Cz-Br-ICz-2** (2.30 g, 3.35 mmol) in *tert*-butylbenzene (*t*-BuPh) (130 mL) at −60 ºC under nitrogen atmosphere. After stirring at 45 ºC for 8 h, pentane was removed in vacuum. After addition of boron tribromide (BBr_3) (3.36 g, 13.40 mmol) at −60 ºC, the reaction mixture was stirred at room temperature for 1 h. *N,N*-Diisopropylethylamine (DIPEA) (3.60 g, 20.10 mmol) was added at 0 ºC, and then the reaction mixture was warmed to room temperature. Next, after stirring at 140 ºC for 12 h, the reaction mixture was cooled to room temperature. Sodium acetate aqueous solution and dichloromethane were added to the reaction mixture for extraction, and the combined organic layer was condensed in vacuum, and the crude product was purified by column chromatography using a mixed eluent of dichloromethane/petroleum ether (1:6) and then recrystallized from dichloromethane and methanol as a purple powder (0.29 g, 0.47 mmol). Yield: 14%. ^{1}H NMR (500 MHz, Toluene-d_8) δ 8.42 (d, J = 1.8 Hz, 1H), 8.10 (d, J = 7.2 Hz, 1H), 7.99 (d, J

= 1.9 Hz, 1H), 7.87 (d, J = 2.0 Hz, 1H), 7.46 (d, J = 7.4 Hz, 1H), 7.42 (d, J = 8.6 Hz, 1H), 7.34 (d, J = 7.3 Hz, 1H), 7.18 – 7.16 (m, 1H), 6.99 (d, J = 8.2 Hz, 1H), 6.95 – 6.92 (m, 1H), 6.86 (dq, J = 7.9, 4.5, 4.0 Hz, 4H), 6.83 – 6.78 (m, 2H), 1.24 (s, 9H), 1.18 (s, 9H). ESI-MS (M): m/z: 615.46 [M]+ (calcd: 615.59).

1.3. Thermal and Electrochemical Characterization

TA Q500 thermogravimeter was selected to perform the thermogravimetric analysis (TGA) under nitrogen atmosphere at a heating rate of 10 K min^{-1}. BAS 100W Bioanalytical electrochemical work station was used to measure the electrochemical property with platinum disk as working electrode, platinum wire as auxiliary electrode, a porous glass wick Ag/Ag^+ as pseudo reference electrode and ferrocene/ferrocenium as the internal standard. And 0.1 M solution of n-Bu_4NPF_6 which was the supporting electrolyte was utilized to measure the reduction (in anhydrous tetrahydrofuran) potential at a scan rate of 100 mV s^{-1}. The LUMO energy levels of the compounds were calculated according to the formula: E_{LUMO} (eV) = −[4.8 + ($E_{1/2}$(ox/red) − $E_{1/2}$(Fc+/Fc))] eV. The HOMO energy level was estimated from the optical bandgaps calculated from the onset of UV–vis absorption spectrum and LUMO energy level.

1.4. Theoretical Calculations Method

The ground state geometries were fully optimized by B3LYP method including Grimme's dispersion correction with 6-31G(d,p) basis set using Gaussian 16 software package.[1–6] The HOMO and LUMO were visualized with Gaussview 6.0. The excited state properties were calculated by TDDFT with the same theory level as DFT. The charge decomposition analysis (CDA), molecular planarity parameter (MPP), LOL-π analysis and LOL-π color-filled maps were completed with Multiwfn program.[7] The drawing of LOL-π isosurface, electrostatic potential map and the calculation of RMSD were completed with VMD 1.9.4.[8]

1.5. Photophysical Characterization

Shimadzu RF–5301 PC spectrometer and Shimadzu UV–2550 spectrophotometer were adopted to record the PL emission spectra and UV–Vis absorption, respectively. The fluorescence and phosphorescence spectra taken at liquid nitrogen temperature (77 K) were recorded by Ocean Optics QE Pro with a 365 nm Ocean Optics LLS excitation source. Edinburgh FLS920 steady state fluorimeter equipping with an integrating sphere was employed to measure the absolute photoluminescence quantum yields of both solution and films. In the ultrafast transient absorption spectroscopy system (Ultrafast System LLC, Helios Fire), a titanium-sapphire laser amplifier (Coherent Inc., Astrella) was utilized to emit femtosecond pulses at a central

wavelength of 800 nm, a pulse width ~ 35 fs, and a repetition rate of 1 kHz. The oscillator (Coherent Inc., Vitara-S) and the amplifier pump source (Coherent Inc., REVOLUTION 38 SYSTEM) were integrated components of the system. Pump light (365 nm) was provided by the tunable optical parametric amplifier (Coherent Inc., TOPAS Prime). The broadband UV–Vis probe light (420–760 nm) was generated by focusing a small portion of the titanium-sapphire laser fundamental into a static sapphire window. The time delay between the pump and probe pulses was precisely controlled using an automated optical delay line, with 8 ns time window and 14 fs resolution. All samples were prepared as dilute toluene solutions (1×10^{-5} M). The effective optical path in quartz cuvette is 2 mm. Custom designed fiber-coupled alignment-free spectrometer with a 1024-pixel CMOS sensor (spectral response: 200–1000 nm) was used as UV–Vis detector. The measured TA data were processed in Glotaran software based on the R-package TIMP.[9] Four-step sequential model was employed in global target analysis.

1.6. Analysis of Rate Constants

The calculation formulas for the rate constant of fluorescence (k_F), internal conversion (k_{IC}), intersystem crossing (k_{ISC}), TADF (k_{TADF}) and reverse intersystem crossing (k_{RISC}) are expressed as following list:[10–13]

$$k_F = \Phi_F/\tau_F \quad \text{(S1)}$$

$$\Phi_{PL} = k_F/(k_F + k_{IC}) \quad \text{(S2)}$$

$$\Phi_F = k_F/(k_F + k_{IC} + k_{ISC}) \quad \text{(S3)}$$

$$\Phi_{ISC} = k_{ISC}/(k_F + k_{IC} + k_{ISC}) \quad \text{(S4)}$$

$$k_{TADF} = \Phi_{TADF}/(\Phi_{ISC}\ \tau_{TADF}) \quad \text{(S5)}$$

$$k_{RISC} = k_F\ k_{TADF}\ \Phi_{TADF}/(k_{ISC}\ \Phi_F) \quad \text{(S6)}$$

$$\Phi_{TADF}/\Phi_F = (\Phi_{ISC}\ \Phi_{RISC})/(1-\Phi_{ISC}\ \Phi_{RISC}) \quad \text{(S7)}$$

Where Φ_{PL} is the total fluorescence quantum yield, Φ_F is the prompt fluorescent component of Φ_{PL}, Φ_{TADF} is the delayed fluorescent component of Φ_{PL}. τ_F is the lifetime of prompt fluorescence, τ_{TADF} is the lifetime of TADF. k_F is the rate constant of fluorescence, k_{IC} is the rate constant of internal conversion; k_{TADF}, k_{ISC}, k_{RISC} are the rate constant of TADF, intersystem crossing and reverse intersystem crossing, respectively. Φ_{ISC} and Φ_{RISC} are the quantum efficiencies of ISC and RISC process, respectively.

1.7. Device Fabrication and Measurement

The indium tin oxide (ITO) glass substrates with a sheet resistance of 15 Ω per square were cleaned with optical detergent, deionized water, acetone and isopropanol successively, and then treated with plasma for 5 minutes. Subsequently, they were transferred to a vacuum chamber. Under high vacuum (< 9×10^{-5} Pa), the organic materials were deposited onto the ITO glass substrates at a rate of 0.5 Å s^{-1}. After finishing the deposition of organic layers, ITO glass substrates were patterned by a shadow mask with an array of 2.0 mm × 2.5 mm openings. Then LiF and Al were successively deposited at a rate of 0.1 Å s^{-1} and 5 Å s^{-1}, respectively. The EL spectrum, CIE coordinates and luminance intensity of OLEDs were recorded by Photo Research PR655, meanwhile, the current density (*J*) and driving voltage (*V*) were recorded by Keithley 2400. By assuming Lambertian distribution, EQE was estimated according to brightness, electroluminescence spectrum and current density. The materials of device fabrication are provided by Xi'an Polymer Light Technology Corp.

2. Figures and Tables

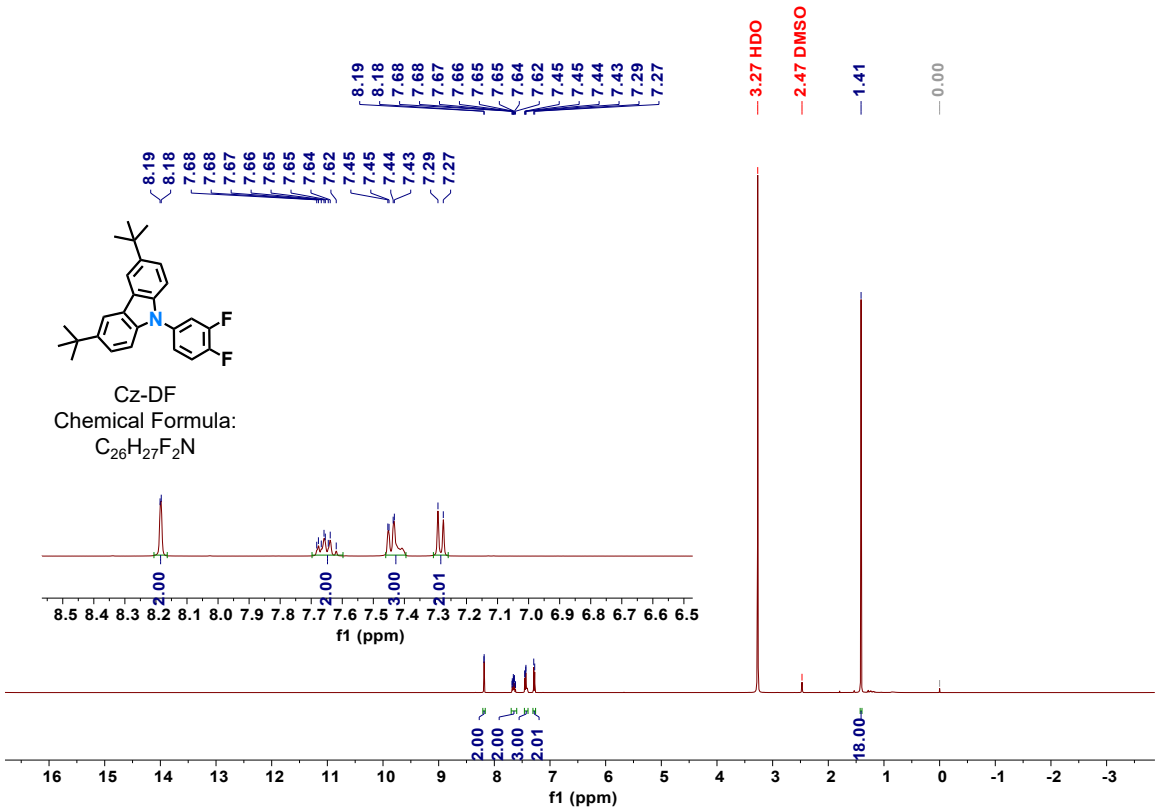

Figure S1. ^{1}H NMR spectrum (500 MHz, DMSO-d_6) of **Cz-DF**.

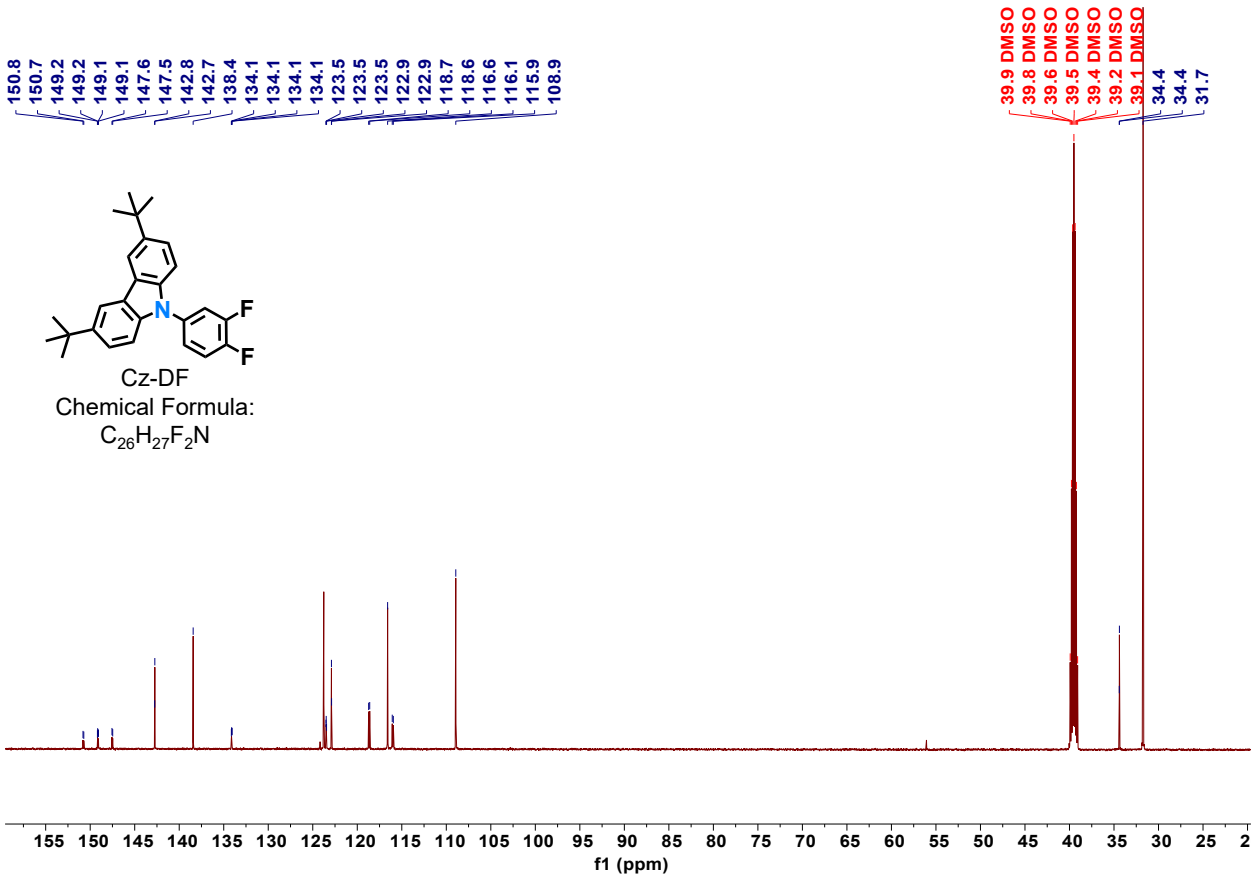

Figure S2. ^{13}C NMR spectrum (151 MHz, DMSO-d_6) of **Cz-DF**.

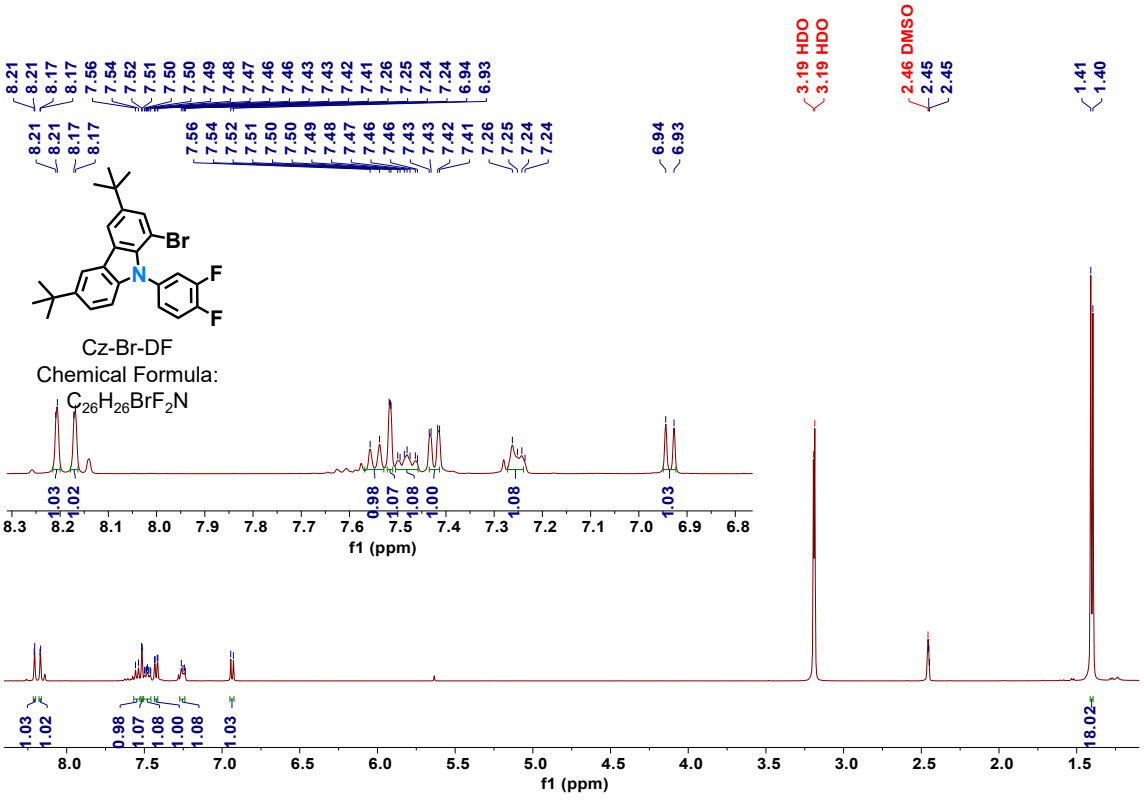

Figure S3. ^{1}H NMR spectrum (500 MHz, DMSO-d_6) of **Cz-Br-DF**.

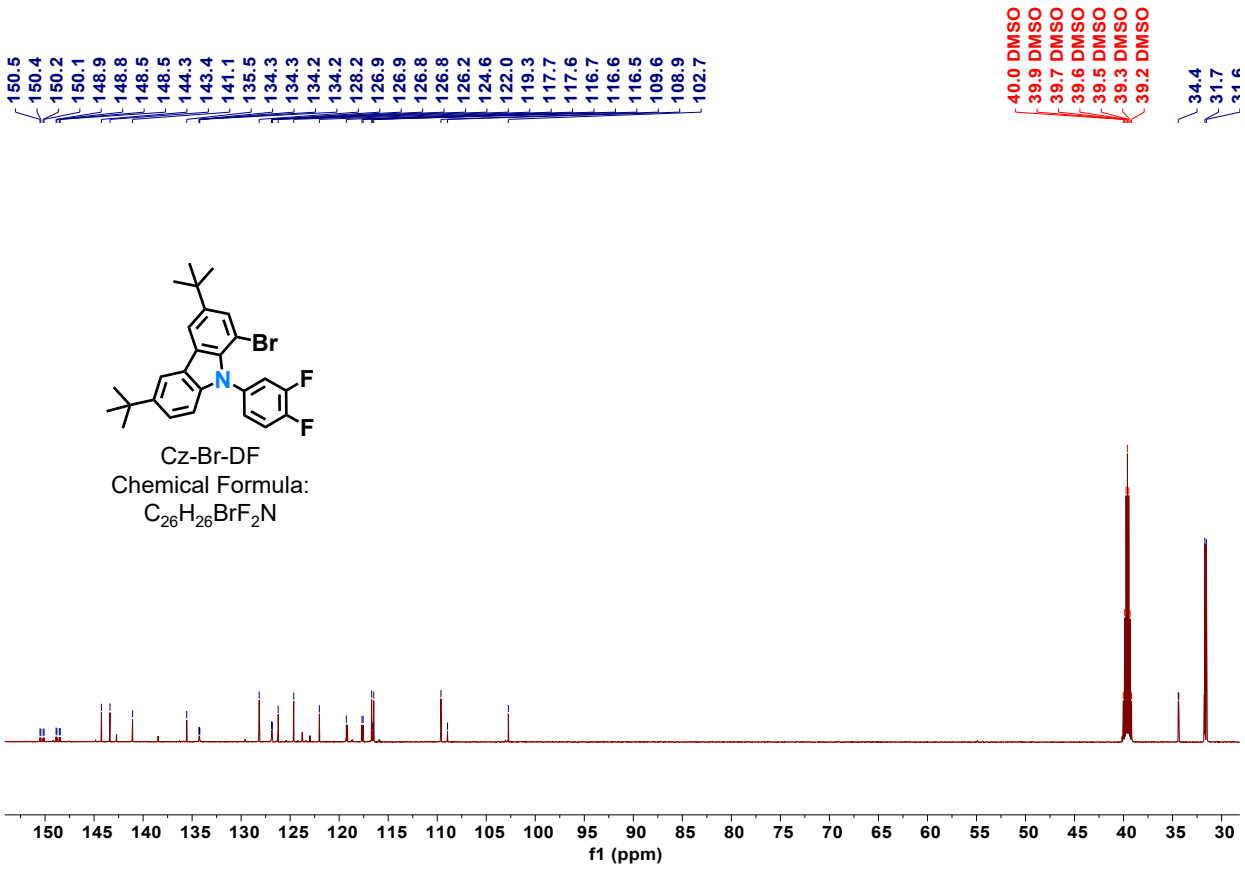

Figure S4. ^{13}C NMR spectrum (151 MHz, DMSO-d_6) of **Cz-Br-DF**.

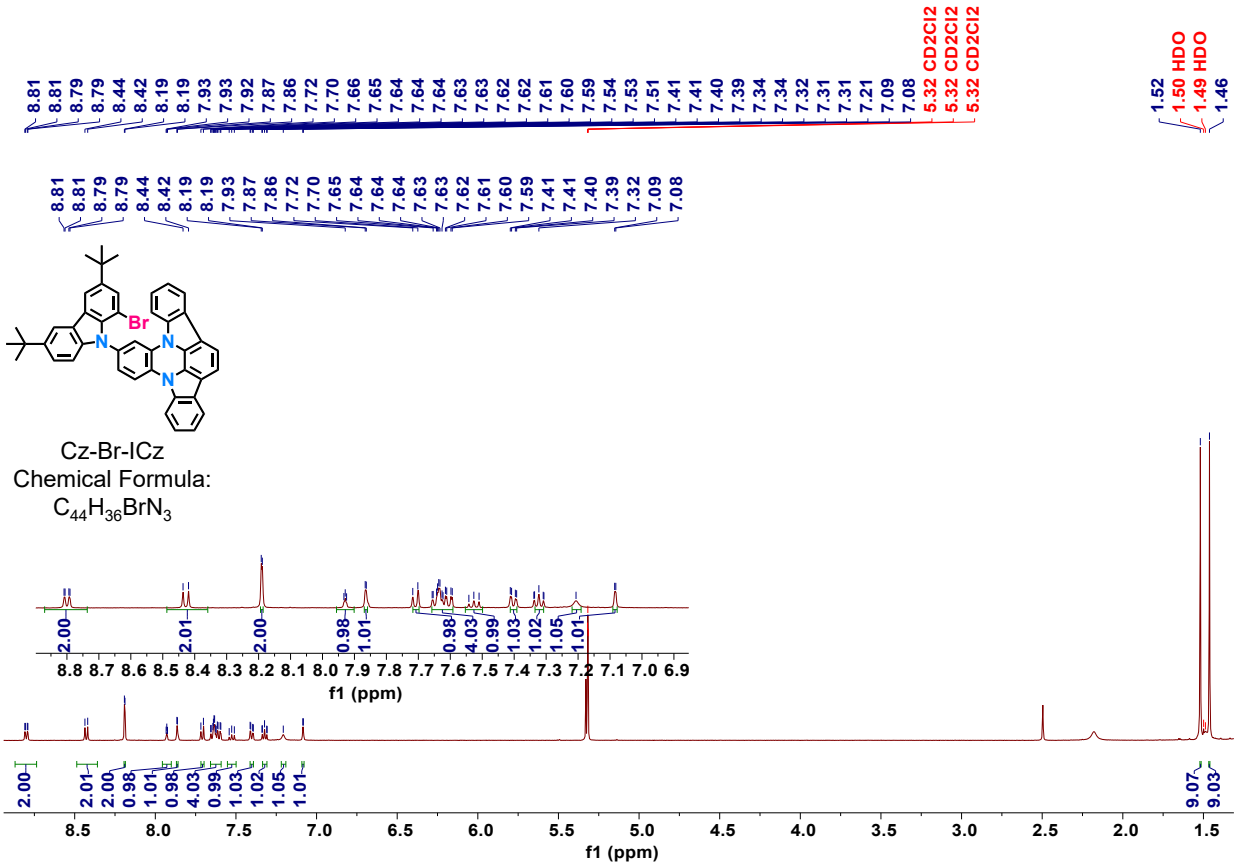

Figure S5. ^{1}H NMR spectrum (500 MHz, CD_2Cl_2-d_2) of **Cz-Br-ICz**.

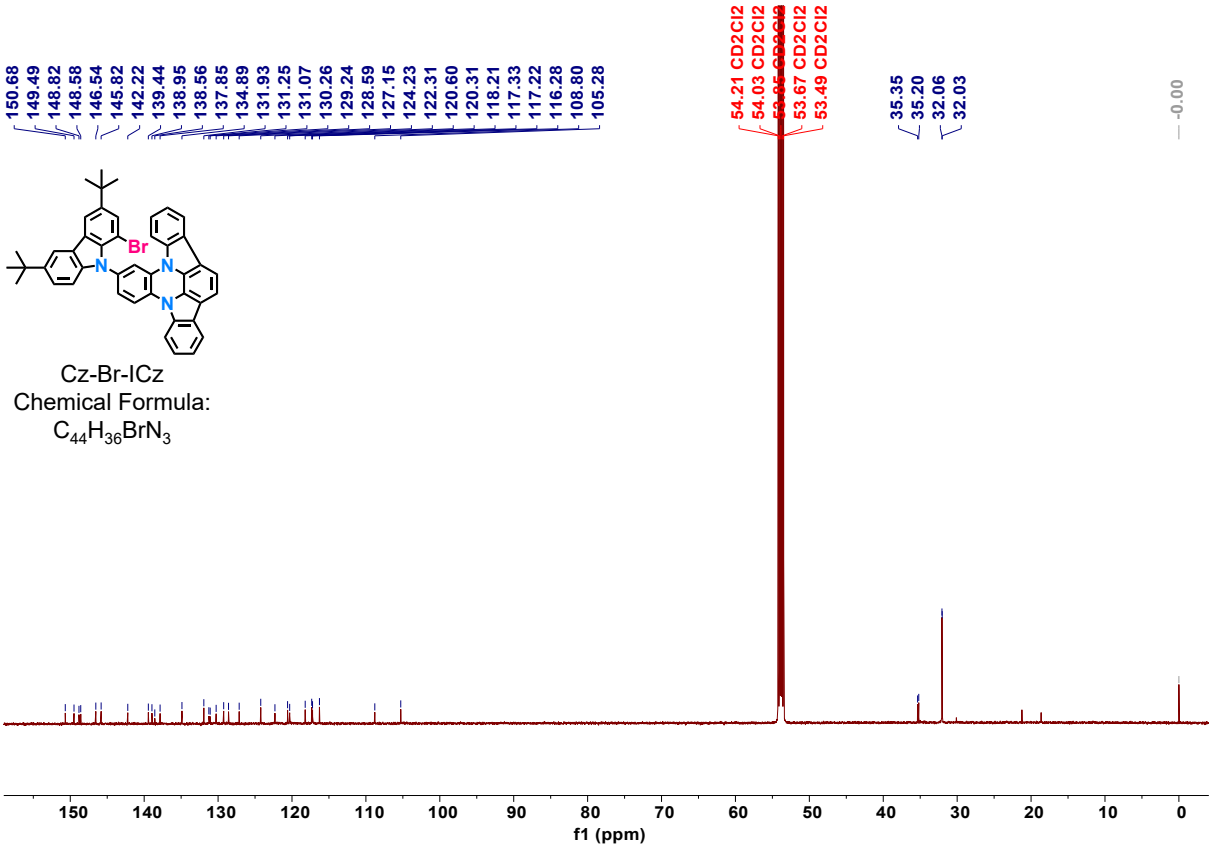

Figure S6. ^{13}C NMR spectrum (151 MHz, CD_2Cl_2-d_6) of **Cz-Br-ICz**.

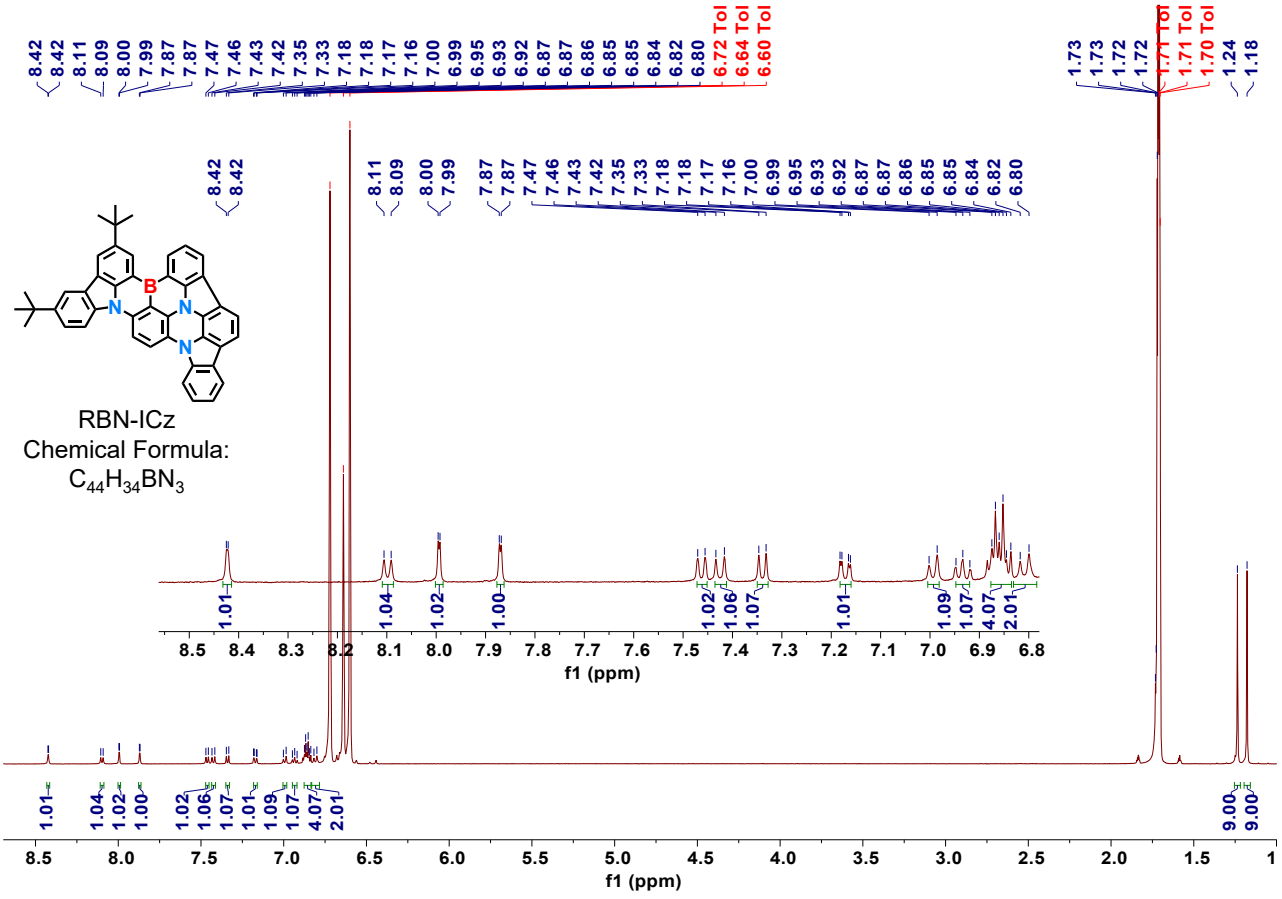

Figure S7. ^{1}H NMR spectrum (500 MHz, Toluene-d_8) of **RBN-ICz**.

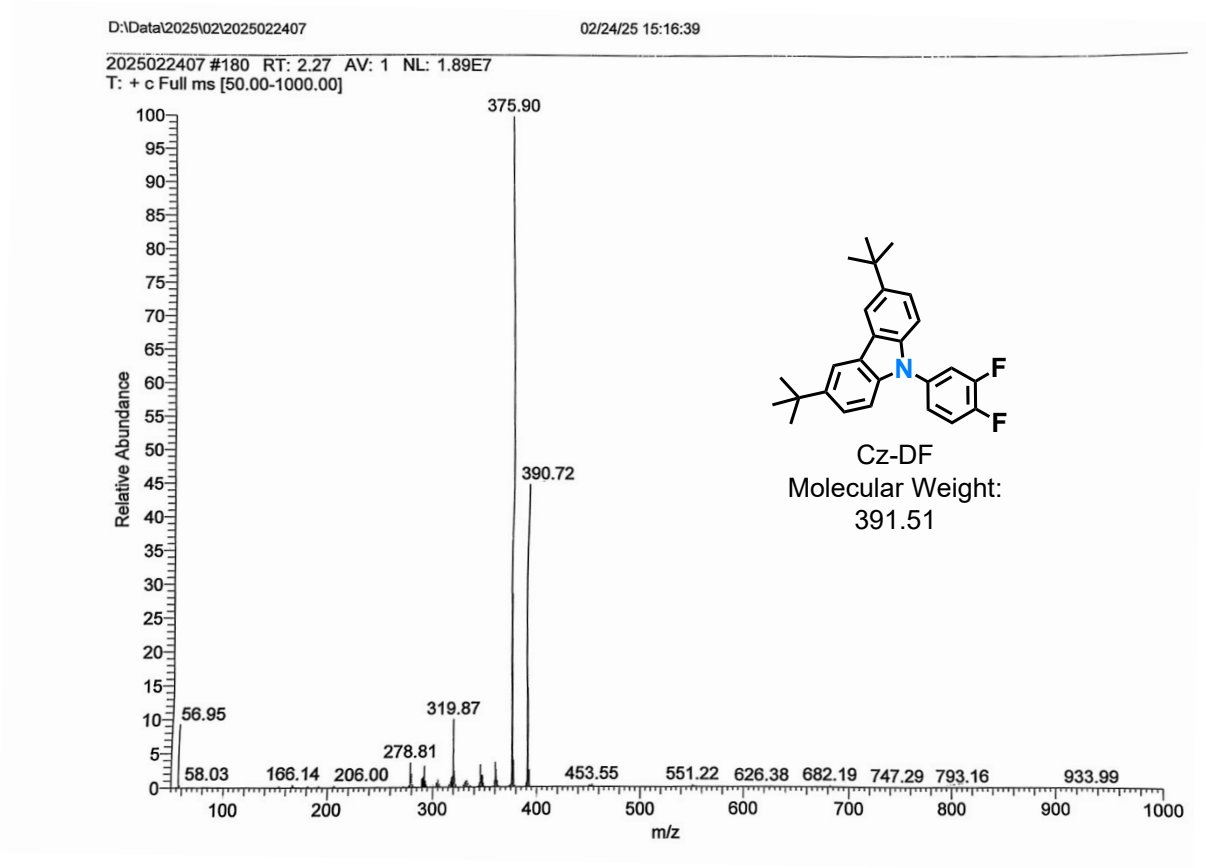

Figure S8. ESI-MS of **Cz-DF**.

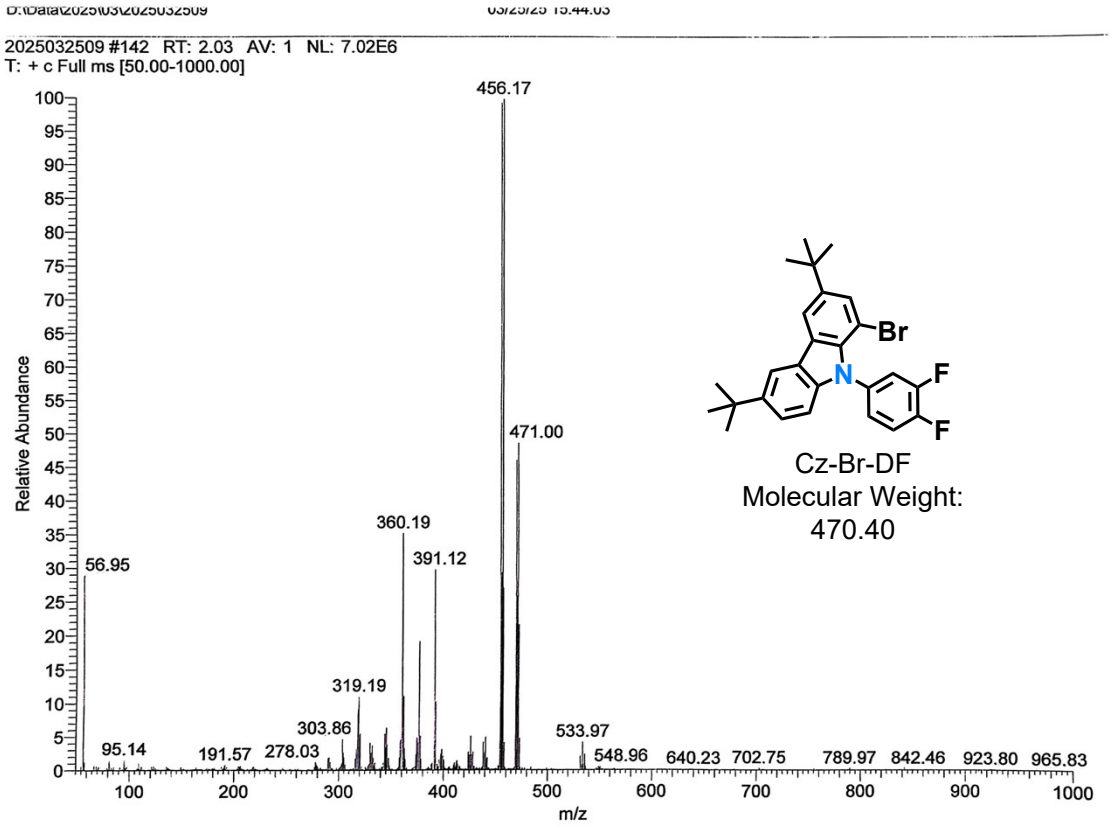

Figure S9. ESI-MS of **Cz-Br-DF**.

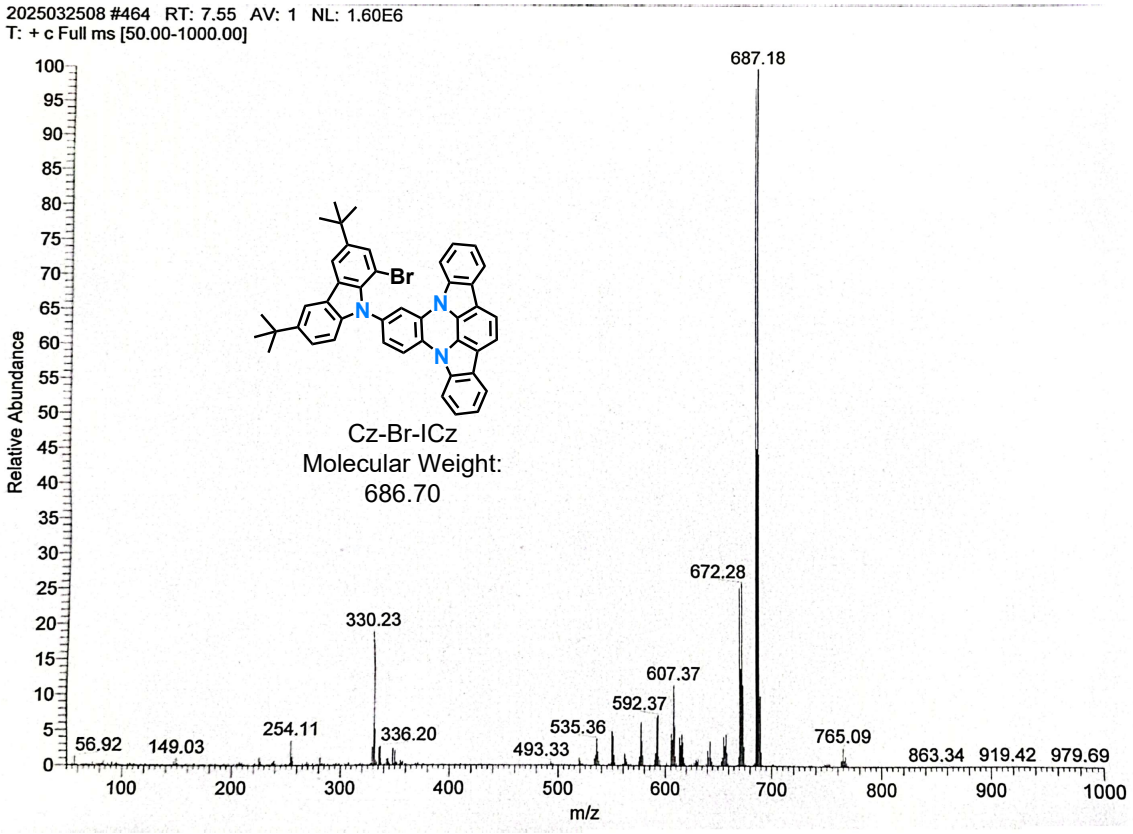

Figure S10. ESI-MS of **Cz-Br-ICz**.

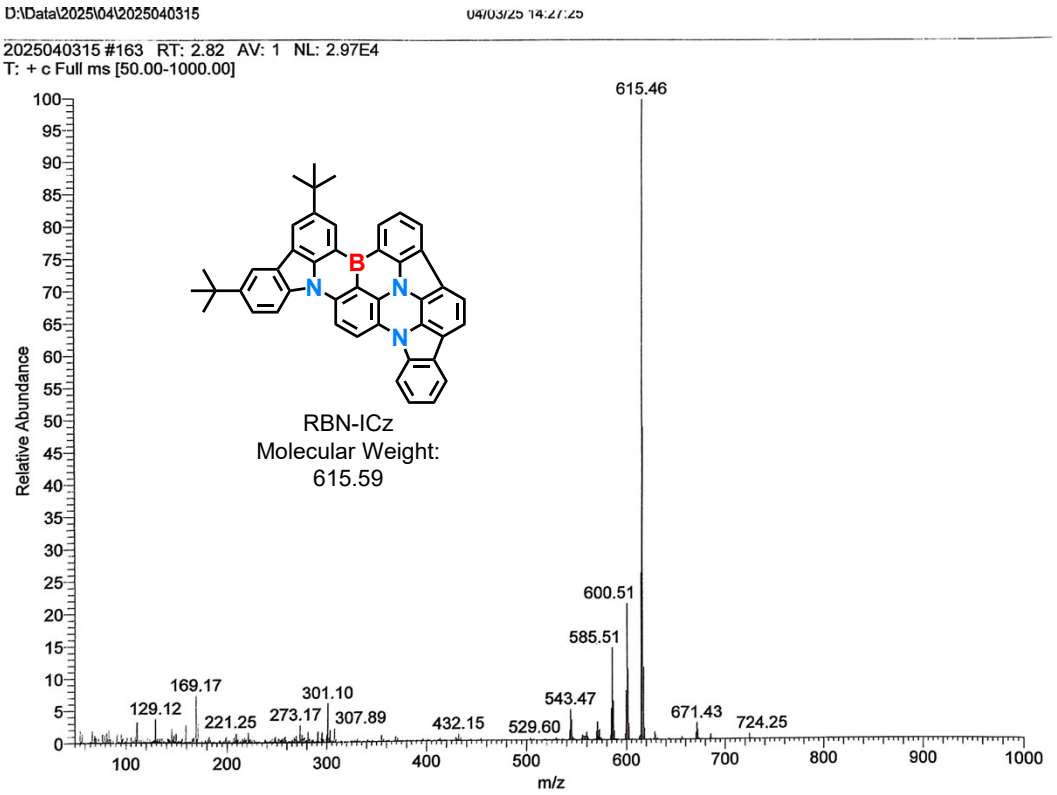

Figure S11. ESI-MS of **RBN-ICz**.

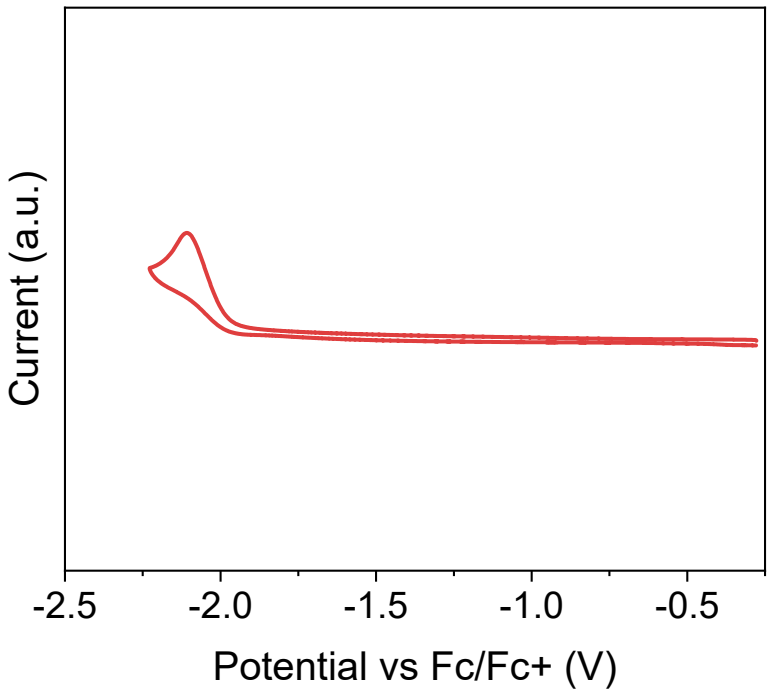

Figure S12. CV curve of **RBN-ICz**.

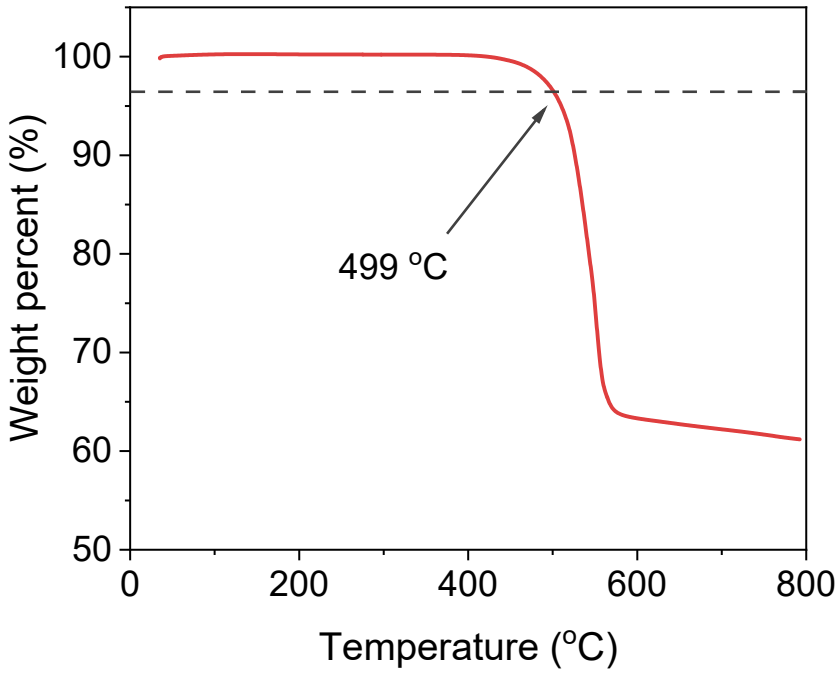

Figure S13. TGA curve of **RBN-ICz**.

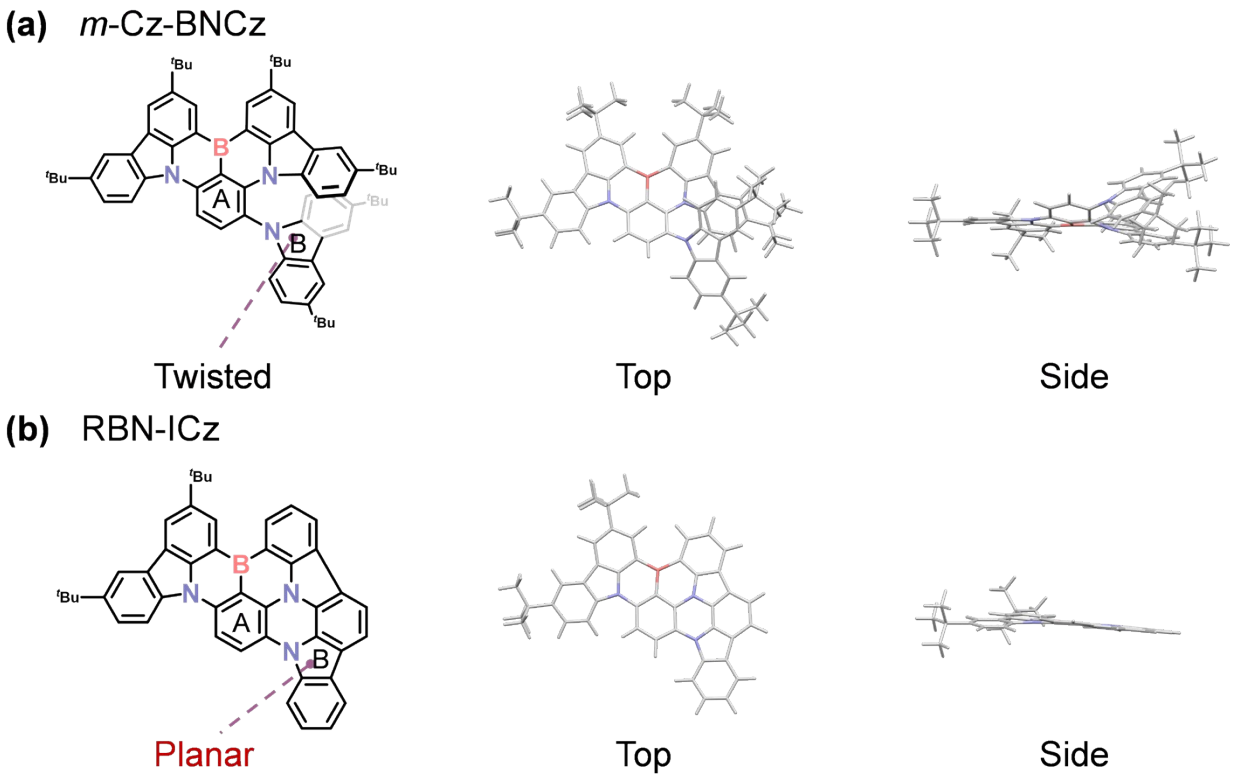

Figure S14. Comparison of the optimized ground-state structures of (a) ***m*-Cz-BNCz** and (b) **RBN-ICz**.

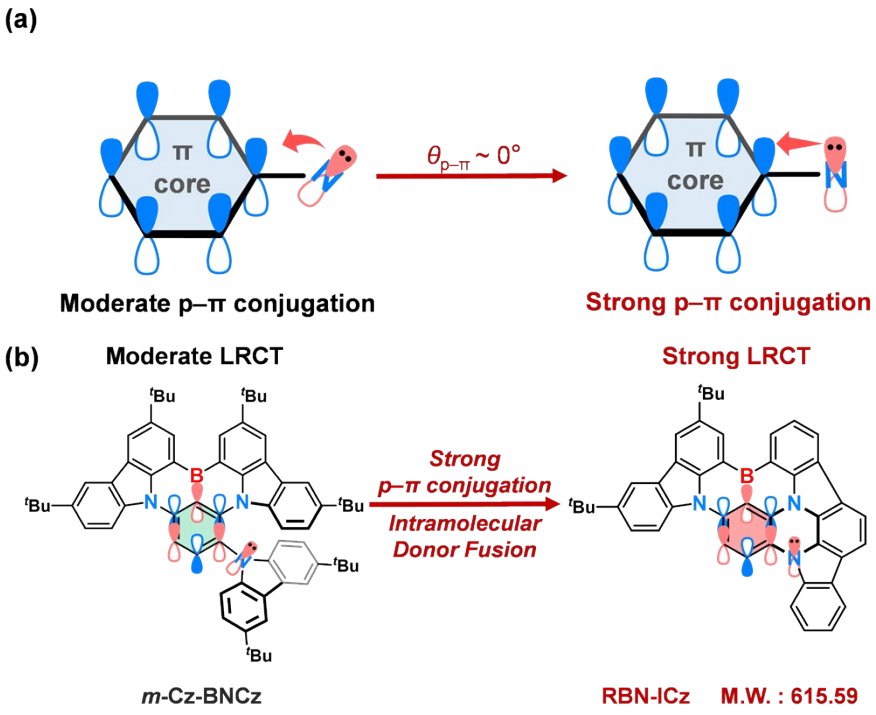

Figure S15. Charge-transfer excited-state regulation based on p–π conjugation of ***m*-Cz-BNCz** and **RBN-ICz**.

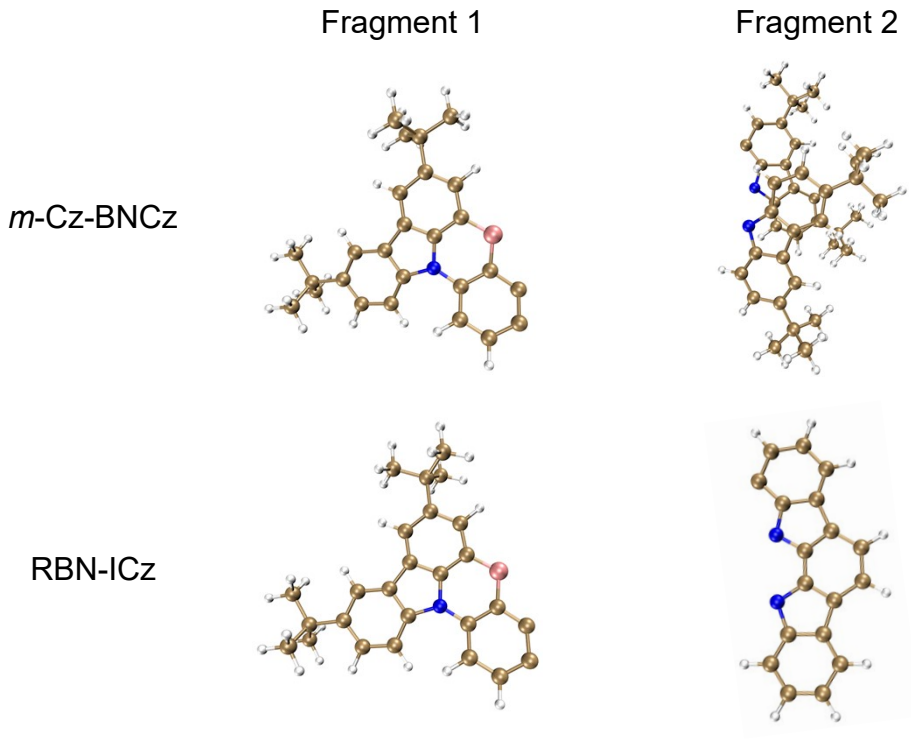

Figure S16. Charge decomposition analysis (CDA) was performed by partitioning each molecule into two fragments: fragment 1 and fragment 2 of ***m*-Cz-BNCz** and **RBN-ICz**.

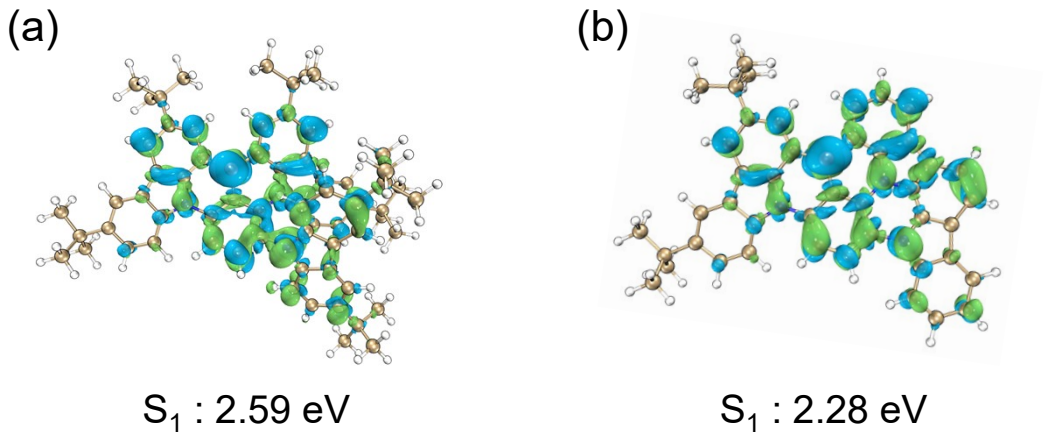

Figure S17. S_1 energies, and difference density plots of S_0 and S_1 states. $\Delta\rho(r) = \rho_{EX}(r) - \rho_{GS}(r)$, $\Delta\rho(r)$ represents the density variation (isovalue = 0.001), and $\rho_{GS}(r)$ and $\rho_{EX}(r)$ are defined as the electronic density associated with the ground and excited states of (a) ***m*-Cz-BNCz** and (b) **RBN-ICz**.

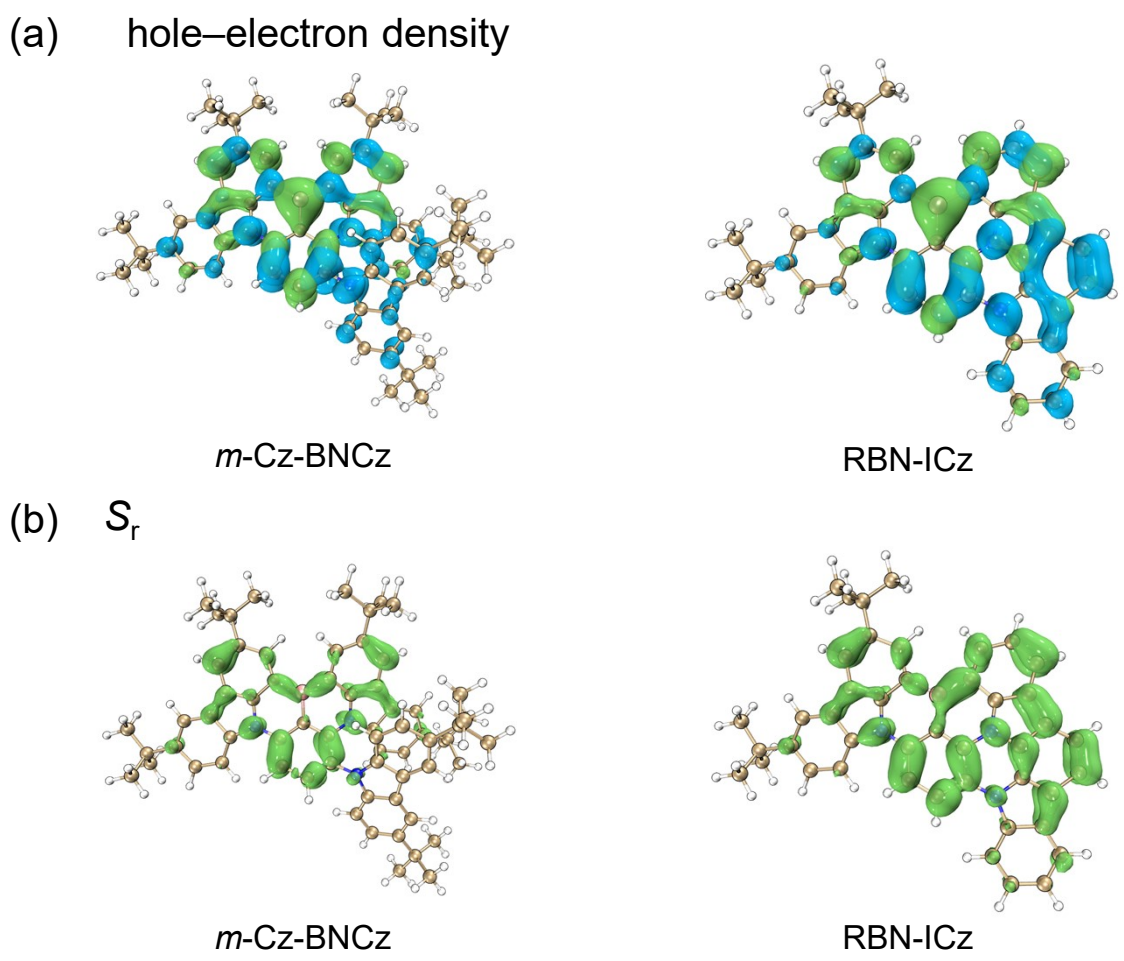

Figure S18. (a) Hole–electron distributions for *m*-Cz-BNCz and RBN-ICz in the S_1. (b) S_r visualizing the spatial correlation between the hole and electron distributions for *m*-Cz-BNCz and RBN-ICz.

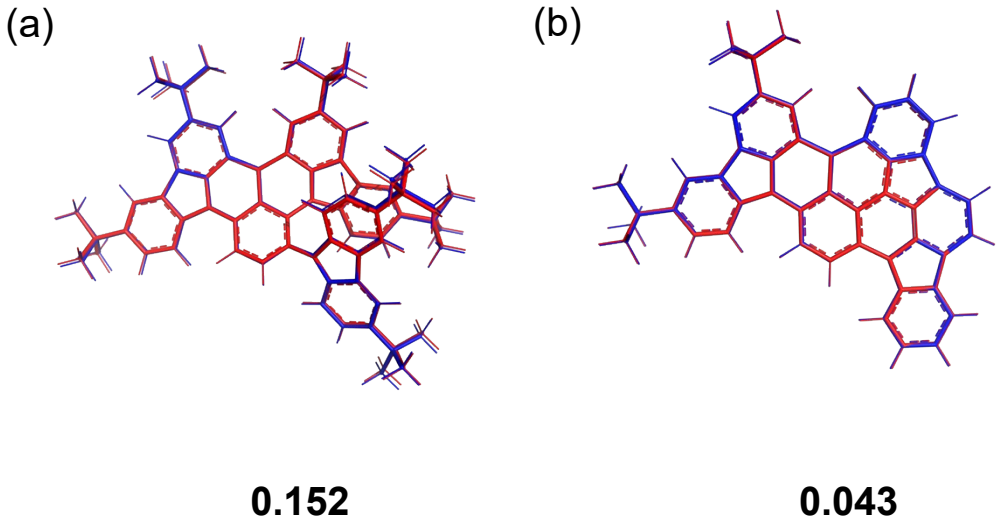

Figure S19. Comparison of the optimized structures of (a) ***m*-Cz-BNCz** and (b) **RBN-ICz** in S_0 (blue) and S_1 (red) and corresponding RMSD.

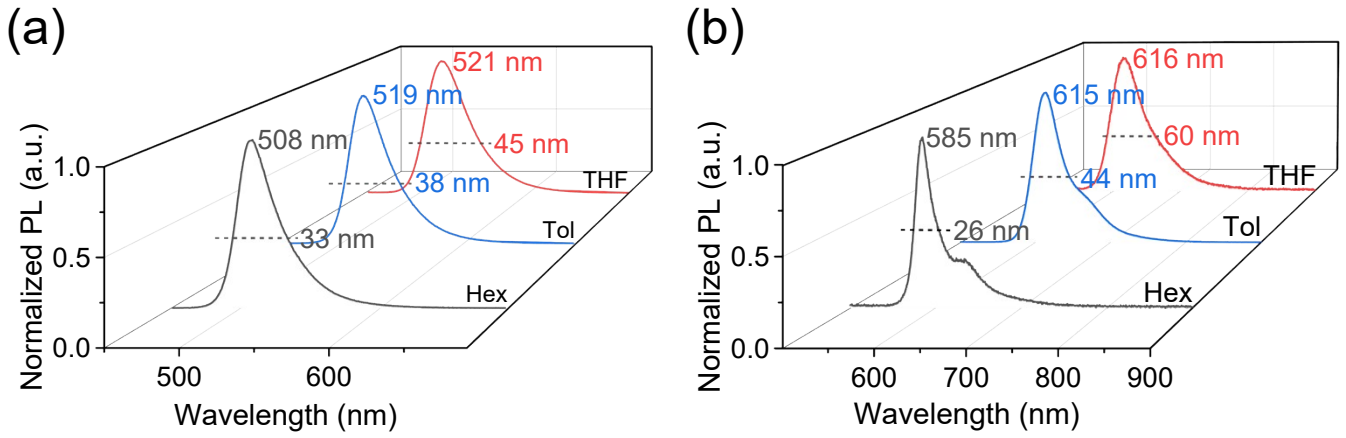

Figure S20. Solvatochromic effects of (a) ***m*-Cz-BNCz**, and (b) **RBN-ICz** measured in different polar solvents (1×10^{-5} M, 298 K).

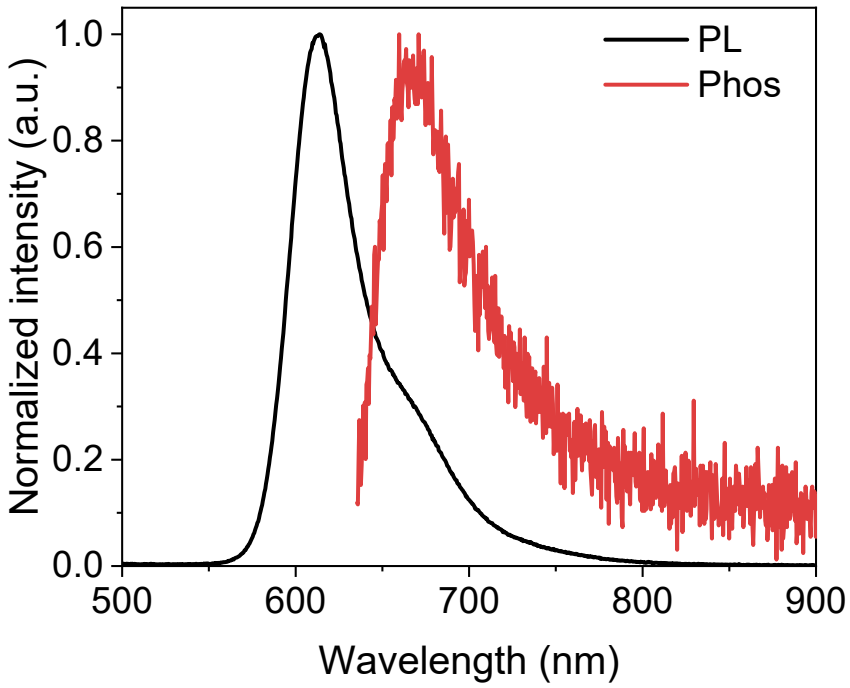

Figure S21. Normalized fluorescence and phosphorescence spectra in toluene solution (1×10^{-5} M, 77 K) of **RBN-ICz** (excited at 365 nm).

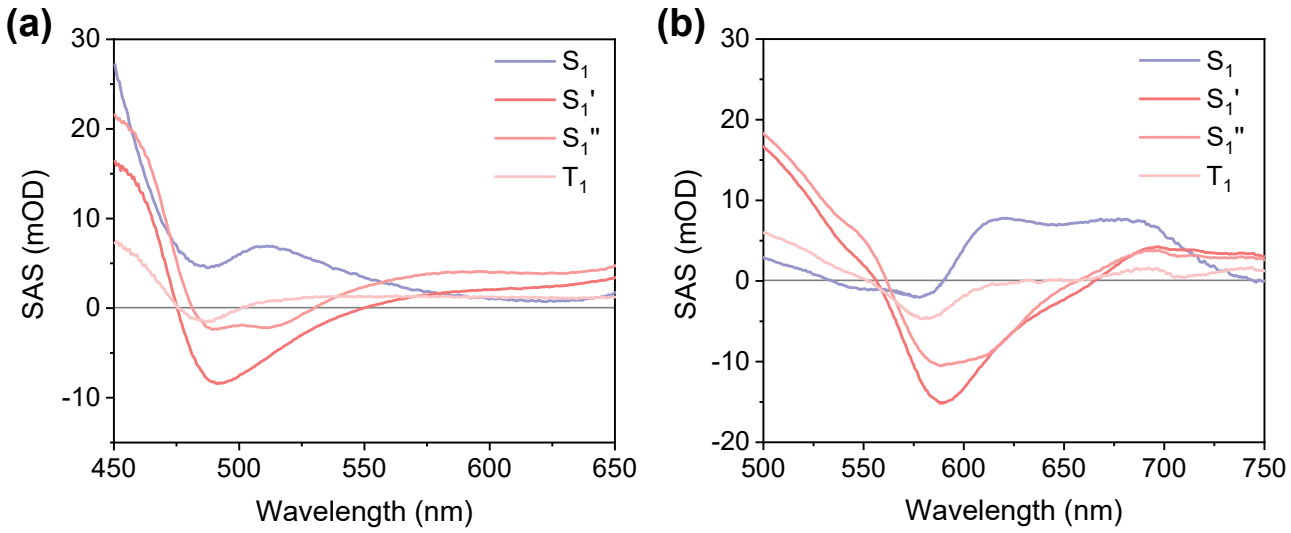

Figure S22. fs-transient absorption dynamics: (a) ***m*-Cz-BNCz** and (b) **RBN-ICz.**

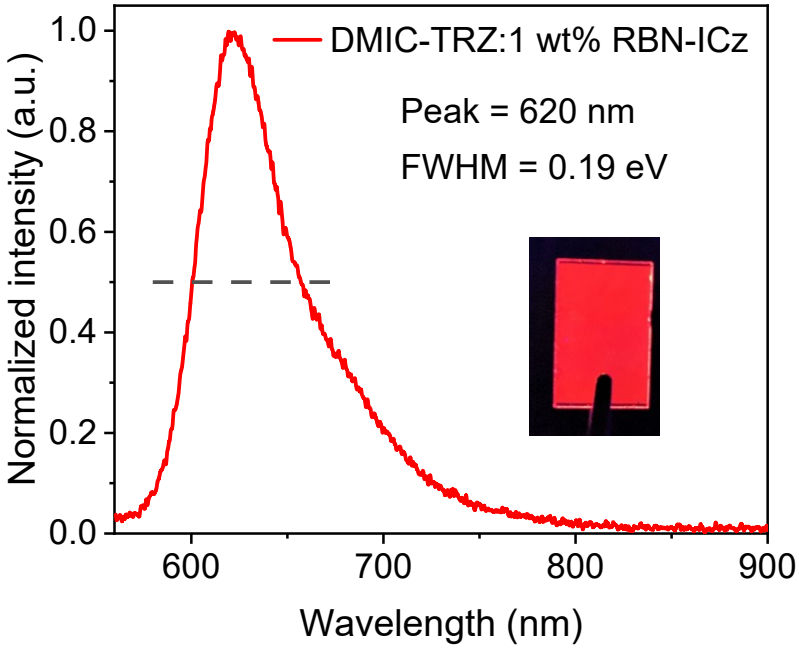

Figure S23. PL spectra of **RBN-ICz** with 1 wt% doping concentration in DMIC-TRZ deposited film (excited at 365 nm. Inset: photograph taken under 365 nm UV light).

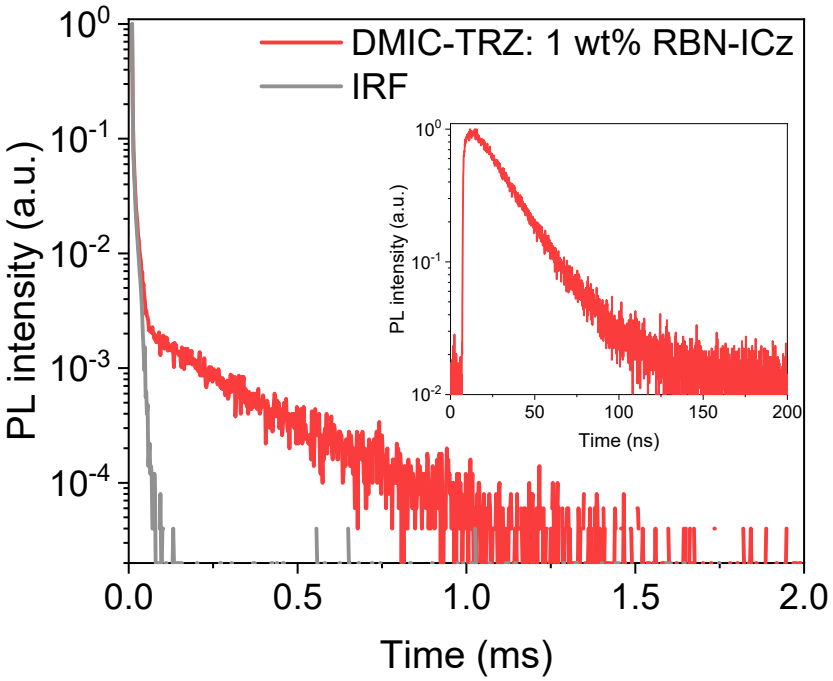

Figure S24. Transient PL decay curve recorded at 298 K and under vacuum atmosphere of **RBN-ICz** with 1 wt% doping concentration in DMIC-TRZ deposited film (excited at 365 nm).

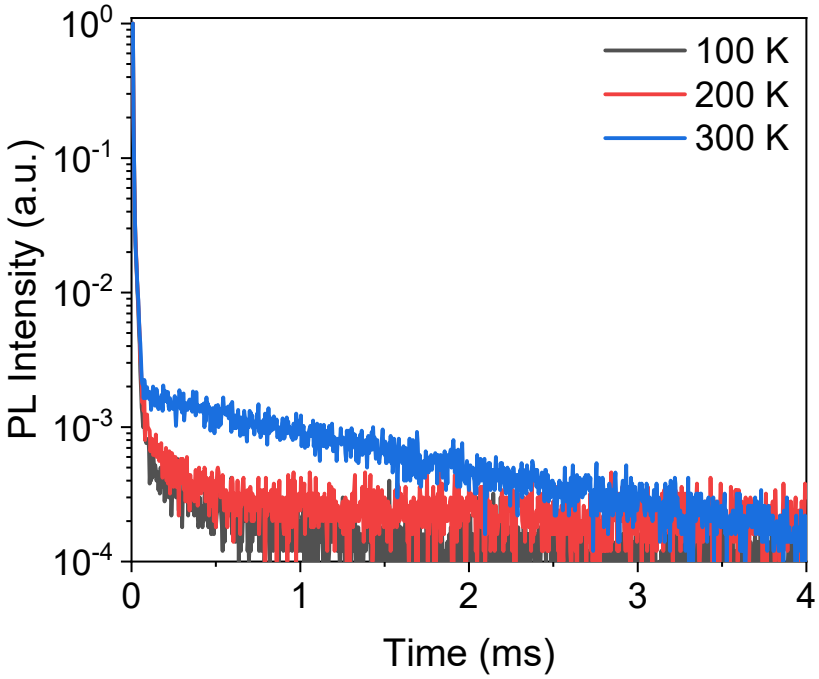

Figure S25. Variable-temperature transient PL decay curves of **RBN-ICz** with 1 wt% doping concentration in DMIC-TRZ deposited film (excited at 365 nm).

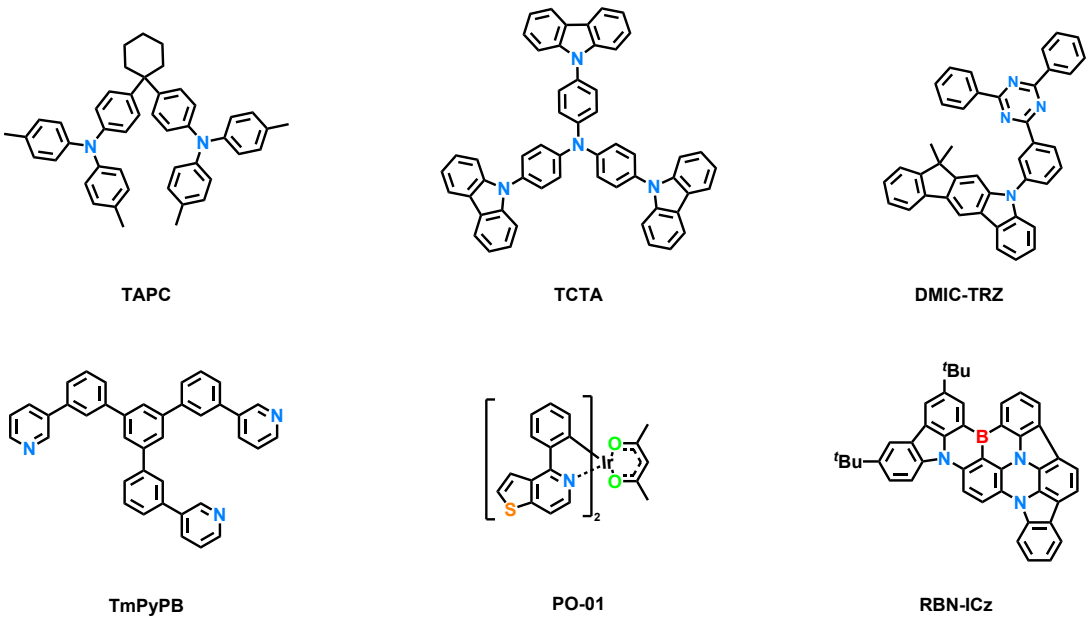

Figure S26. Structures of the materials used in the devices with single host (with/without sensitizer).

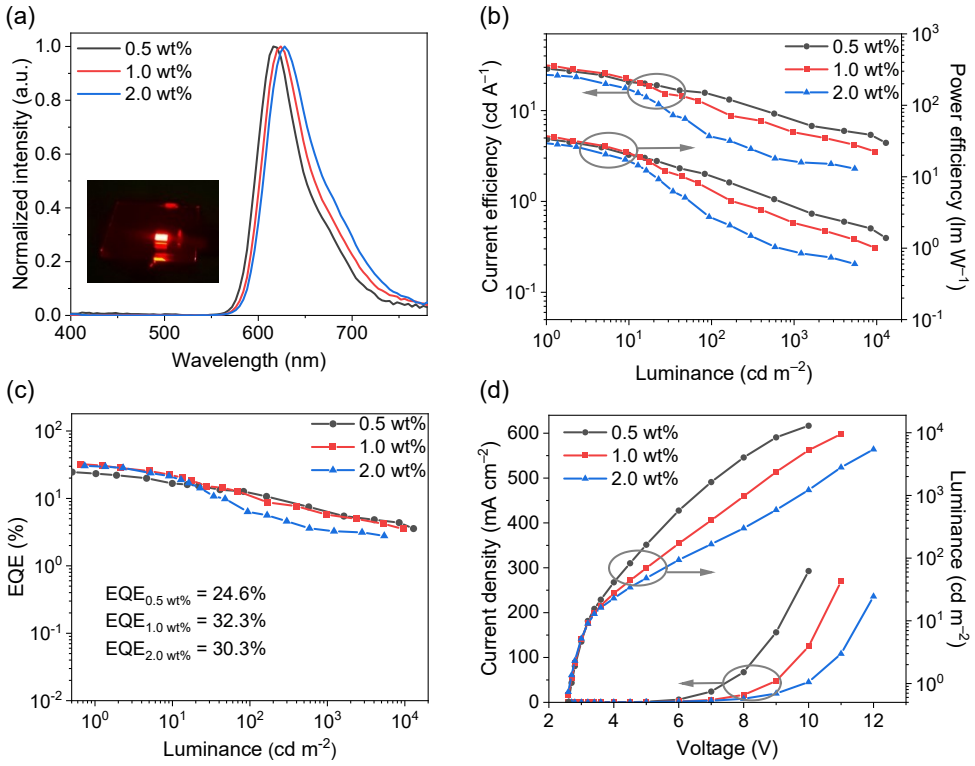

Figure S27. EL characteristics of **RBN-ICz**-based devices with the configuration of [ITO/TAPC (50 nm)/TCTA (5 nm)/DMIC-TRZ: x wt% **RBN-ICz** (30 nm)/TmPyPB (30 nm)/LiF (1 nm)/Al (100 nm) (x = 0.5, 1.0 and 2.0)]. (a) EL spectra. (b) CE–*L* and PE–*L* curves. (c) EQE–*L* curves. d) *J*–*V*–*L* curves.

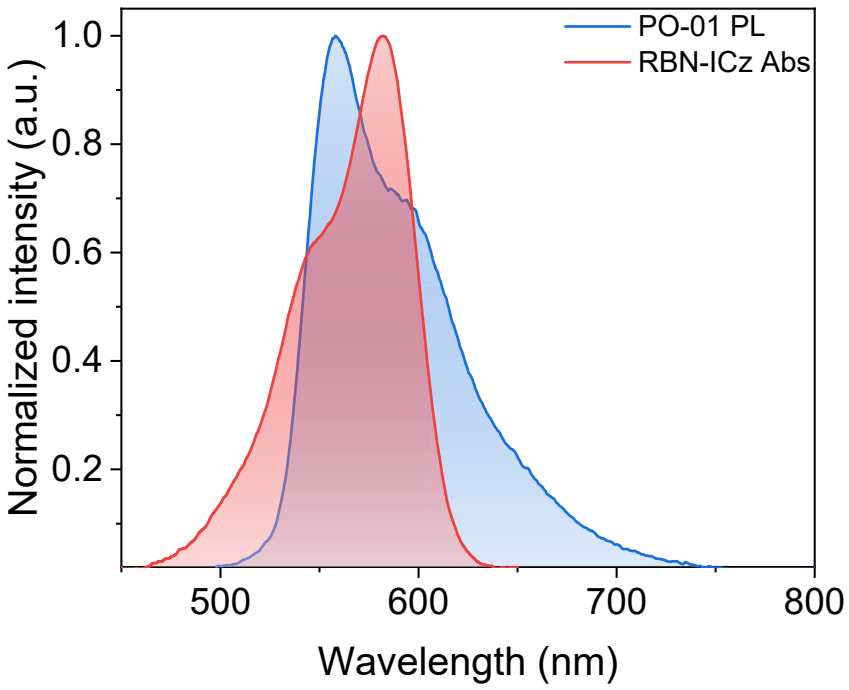

Figure S28. UV–vis absorption spectrum of **RBN-ICz** (toluene, 1 × 10^{-5} M, 298 K) and PL spectrum of PO-01 (toluene, 1 × 10^{-5} M, 298 K, excited at 365 nm).

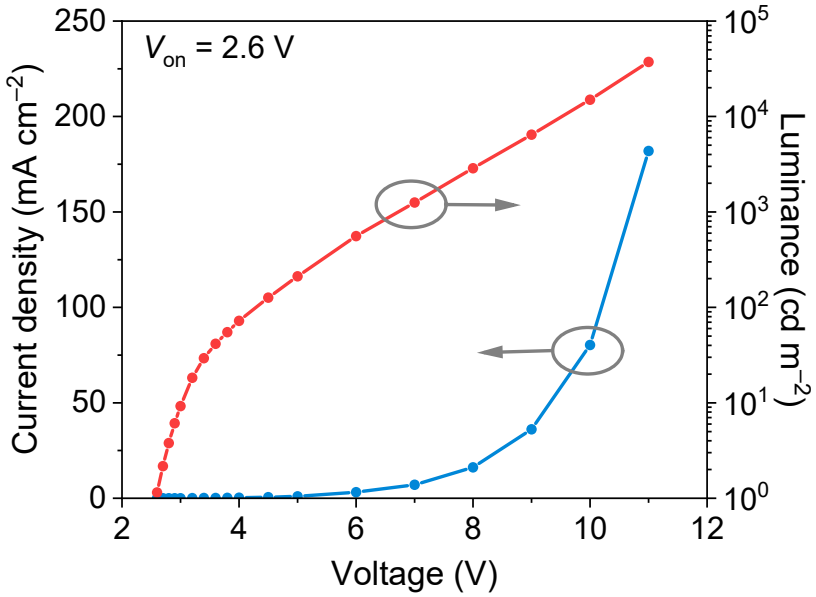

Figure S29. *J–V–L* curves of **RBN-ICz**-based devices with the configuration of [ITO/TAPC (50 nm)/TCTA (5 nm)/DMIC-TRZ: 25 wt% PO-01: 1 wt% **RBN-ICz** (30 nm)/TmPyPB (30 nm)/LiF (1 nm)/Al (100 nm)].

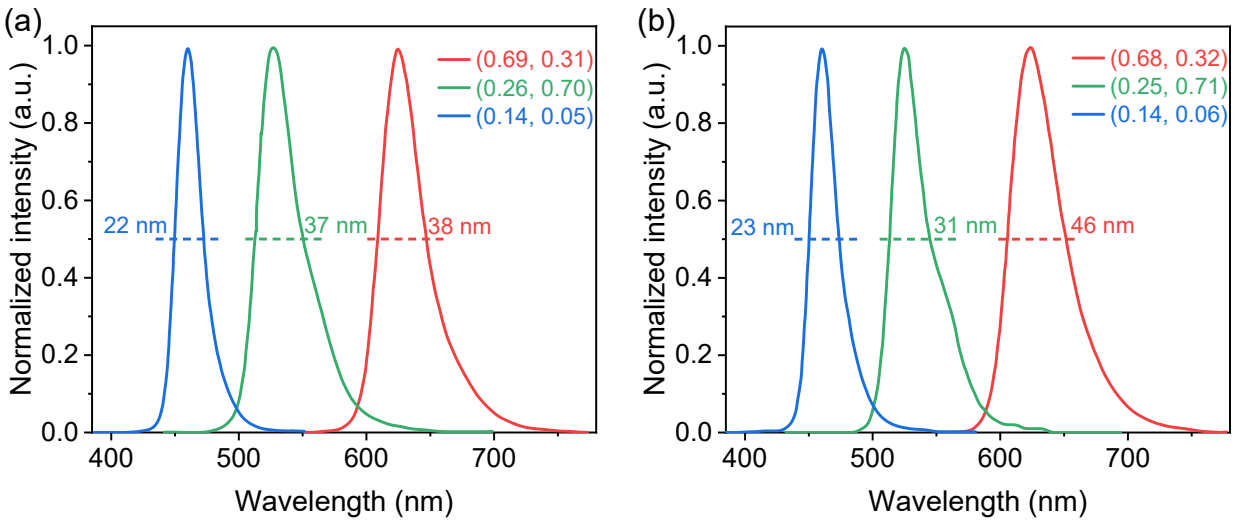

Figure S30. Normalized RGB emission spectra of the latest smartphone based on (a) Samsung AMOLED and (b) Creative Life (TCL) AMOLED.

Table S1. Summary of PL spectra data in different polar solvents of ***m*-Cz-BNCz** and **RBN-ICz**.

Compound	Hexane [PL[a]/FWHM[b]]	Toluene [PL[a]/FWHM[b]]	Tetrahydrofurane [PL[a]/FWHM[b]]
***m*-Cz-BNCz**	508 nm/33 nm	519 nm/38 nm	521 nm/45 nm
RBN-ICz	585 nm/26 nm	615 nm/44 nm	616 nm/60 nm

[a] PL peak wavelength. [b] Full-width at half-maximum.

Table S2. Summary of PL spectrum data of **RBN-ICz** with 1 wt% doping concentration in DMIC-TRZ deposited film.

compound	λ_{em}[a] [nm]	FWHM[b] [nm/eV]	Φ_{PL}[c] [%]
RBN-ICz	620	59/0.19	96.3

[a] PL peak wavelength. [b] Full-width at half-maximum. [c] Absolute photoluminescence quantum yield.

Table S3. Summary of photophysical data of **RBN-ICz** with 1 wt% doping concentration in DMIC-TRZ deposited film.

Emitter	Φ_{PL}[a] [%]	Φ_F[b] [%]	Φ_{TADF}[c] [%]	τ_F[d] [ns]	τ_{TADF}[e] [μs]	k_F[f] [10^8 s^{-1}]	k_{ISC}[g] [10^7 s^{-1}]	k_{RISC}[h] [10^3 s^{-1}]
RBN-ICz	96.3	70.7	25.6	3.33	209.9	3.0	8.8	6.7

[a] The total photoluminescence quantum yield (Φ_{PL}). [b] The prompt fluorescent (Φ_F) component of Φ_{PL}. [c] The delayed fluorescent (Φ_{TADF}) component of Φ_{PL}. [d] The lifetime of prompt fluorescence (τ_F). [e] The lifetime of delayed fluorescence (τ_{TADF}). [f] The rate constant of prompt fluorescence (k_F). [g] The rate constant of intersystem crossing (k_{ISC}). [h] The rate constant of reverse intersystem crossing (k_{RISC}).

Table S4. Summary of EL data of devices (single host: DMIC-TRZ) based on emitter **RBN-ICz** with different doping concentration.

x wt%	λ_{em}[a] [nm]	FWHM[b] [nm]/[eV]	CIE(x, y)[c]	V_{on}[d] [V]	L_{max}[e] [cd m^{-2}]	CE_{max}[f] [cd A^{-1}]	PE_{max}[g] [lm W^{-1}]	EQE[h] [%]
0.5	616	54/0.17	(0.66, 0.33)	2.6	12940	30.4	36.7	24.6
1.0	620	57/0.18	(0.67, 0.33)	2.6	9545	32.5	39.2	32.3
2.0	628	64/0.20	(0.68, 0.32)	2.6	5429	25.1	30.2	30.3

[a] EL peak wavelength. [b] Full-width at half-maximum. [c] Commission Internationale de L'Eclairage coordinates (value taken at 100 cd m^{-2}). [d] Turn-on voltage at 1 cd m^{-2}. [e] Maximum luminance. [f] Maximum current efficiency. [g] Maximum power efficiency. [h] Maximum external quantum efficiency, respectively.

Table S5. Summary of OLED performance ($CIE_x \geq 0.54$) employing representative red MR-TADF emitters.

Emitter	λ_{em}[a] [nm]	FWHM[b] [nm/eV]	CIE (x, y)[c]	CE_{max}[f] [cd A^{-1}]	PE_{max}[g] [lm W^{-1}]	EQE_{max}[h] [%]	M.W.[i]	Reference
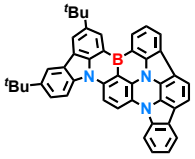 **RBN-ICz**	620	57/0.18	(0.67, 0.33)	32.5	39.2	32.3	615	This work
RBN-ICz*	624	59/0.19	(0.67, 0.33)	32.3	39.5	34.1	615	This work

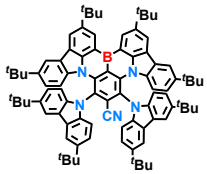 **CNCz-BNCz***	583	49/0.18	(0.54, 0.46)	101.3	117.8	33.7	1220	[14]
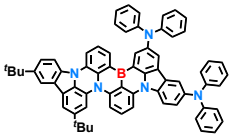 **BNIP-CzDPA**	584	62/0.23	(0.54, 0.45)	82.9	93.0	32.4	952	[15]
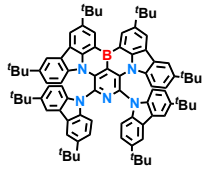 **Py-Cz-BN**	587	54/0.19	(0.55, 0.45)	–	–	29.6	1197	[16]
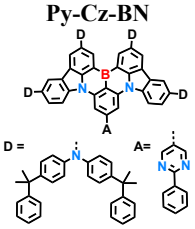 **BN-R3**	585	43/0.16	(0.55, 0.45)	57.1	68.3	19	2185	[17]
BN-R3*	587	44/0.16	(0.55, 0.44)	55.5	66.0	20.4	2185	[17]
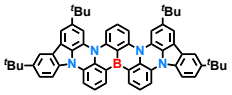 **TCZ-F-DABNA**	588	61/0.22	(0.54, 0.44)	106.7	108.1	39.2	819	[18]
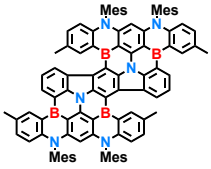 **B4N6-Me**	588	26/0.10	(0.57, 0.42)	87.2	94.4	31.7	1333	[19]
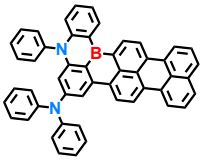 **BP-2DPA**	605	42/0.14	(0.62, 0.38)	14.0	–	11.3	670	[20]
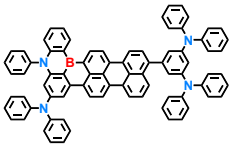 **BP-4DPA**	617	44/0.14	(0.63, 0.36)	13.8	–	15.1	1081	[20]
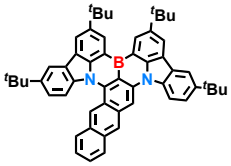 **AN-BN**	608	54/0.18	(0.63, 0.37)	62.6	56.1	27.3	740	[21]
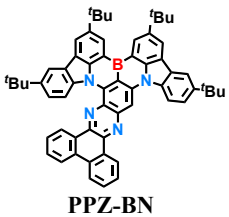 **PPZ-BN**	613	55/0.18	(0.66, 0.34)	34.9	34.6	26.9	843	[22]

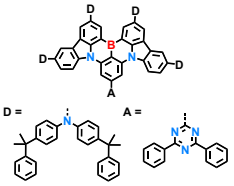 **BN-R**	617	47/0.15	(0.65, 0.34)	30.2	31.2	22.0	2262	[23]
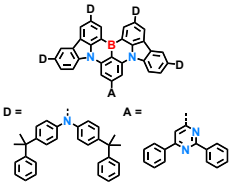 **BN-R1**	610	44/0.15	(0.64, 0.36)	33.5	39.0	20.7	2261	[23]
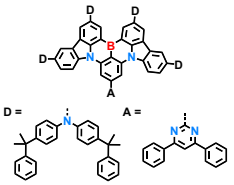 **BN-R2**	601	40/0.14	(0.62, 0.38)	44.4	54.5	21.1	2261	[23]
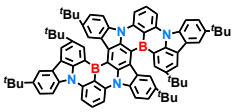 **BBCz-R**	616	26/0.09	(0.67, 0.33)	–	–	22.0	1091	[24]
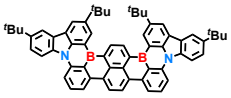 **Na-dBN**	621	38/0.12	(0.66, 0.34)	31.2	34.0	25.2	851	[25]
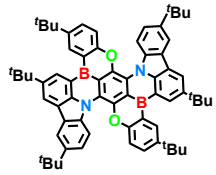 **BNO1**	610	39/0.13	(0.64, 0.34)	59.4	66.7	35.6	945	[26]
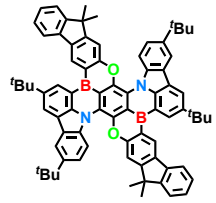 **BON2**	618	39/0.13	(0.65, 0.35)	46.5	52.2	34.4	1065	[26]
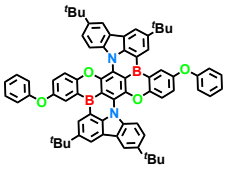 **BON3**	625	40/0.13	(0.66, 0.34)	43.4	48.7	36.1	1017	[26]
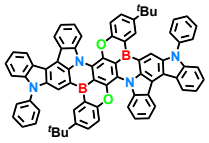 **BNNO**	643	42/0.13	(0.71, 0.29)	25.2	24.1	34.4	1050	[27]
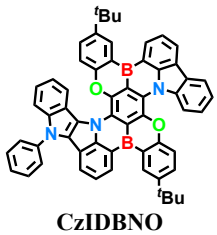 **CzIDBNO**	643	47/0.14	(0.70, 0.30)	20.2	24.1	32.5	836	[28]

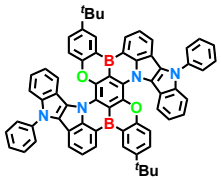 **IDIDBNO**	671	49/0.14	(0.70, 0.30)	8.4	8.8	27.2	951	[28]
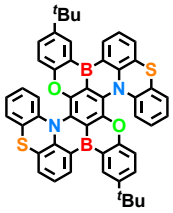 **PTZBNO**	617	59/0.19	(0.63, 0.35)	20.3	26.6	13.6	785	[29]
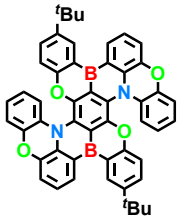 **PXZBNO**	630	53/0.17	(0.66, 0.35)	9.7	10.9	11.8	752	[29]
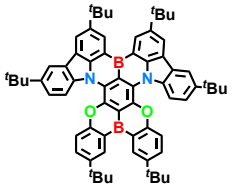 **DB3**	606	35/0.12	(0.63, 0.36)	31.1	40.7	17.8	945	[30]
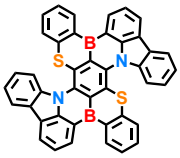 **DBNS**	613	66/0.22	(0.64, 0.34)	7.2	–	5.8	53.7	[31]
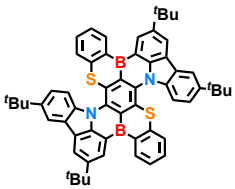 **DBNS-tBu**	616	65/0.20	(0.65, 0.34)	9.2	–	7.8	865	[31]
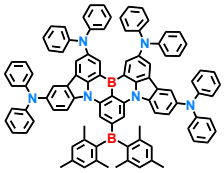 **BNCZ-DPAB**	623	52/0.17	(0.65, 0.35)	41.8	34.6	31.4	1333	[32]
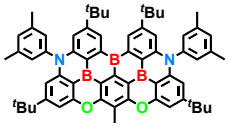 **Δ-DABNA-TB**	624	42/0.13	(0.66, 0.34)	30.1	24.7	23.3	915	[33]
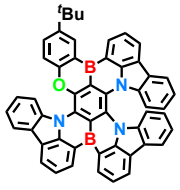 **RBNO1**	632	53/0.17	(0.69, 0.31)	26.6	34.8	33.1	737	[34]

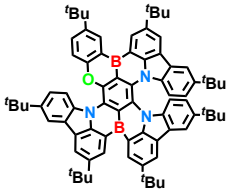 **RBNO2**	645	49/0.15	(0.70, 0.30)	18.5	20.7	34.7	1074	[34]
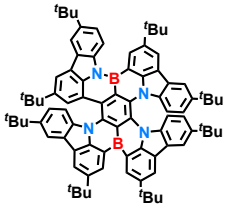 **RBNN**	617	48/0.16	(0.67, 0.33)	117.5	153.7	36.6	1203	[35]
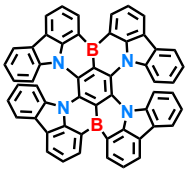 **R-BN**	663	48/0.14	(0.72, 0.28)	–	–	25.6	754	[36]
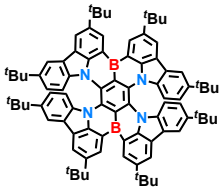 **R-TBN**	686	48/0.13	(0.72, 0.28)	–	–	24.7	1203	[36]
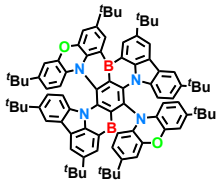 **PXZ-R-BN**	693	59/0.15	–	–	–	29.3	1235	[37]
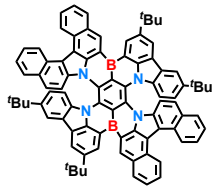 **BCz-R-BN**	713	56/0.14	–	–	–	24.2	1179	[37]
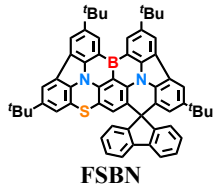 **FSBN**	624	58/0.18	(0.67, 0.33)	43.3	50.1	37.5	832	[38]
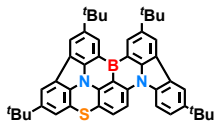 **S-BN**	600	58/0.20	(0.61, 0.39)	74.5	93.6	39.9	670	[39]
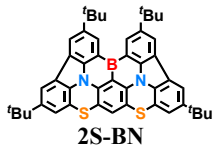 **2S-BN**	676	62/0.16	(0.70, 0.28)	4.2	4.4	29.3	700	[39]

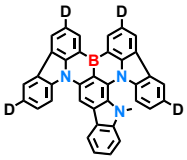 **BNTPA**	617	48/0.15	(0.663, 0.337)	70.8	76.7	43.3	1180	[40]
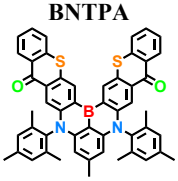 **2TXBN**	591	35/0.12	(0.57, 0.42)	69.0	76.0	31.0	786	[41]
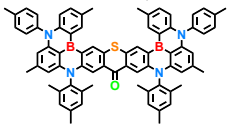 **BNTXBN**	600	41/0.14	(0.61, 0.40)	25.2	26.3	11.8	1065	[41]
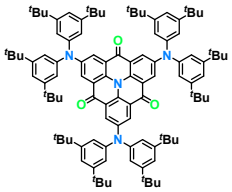 ***m*BDPA-TOAT**	599	45/0.15	(0.61, 0.39)	37.1	36.4	17.3	1498	[42]
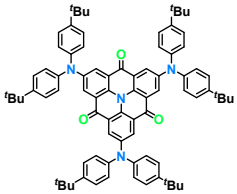 ***p*BDPA-TOAT**	603	62/0.20	(0.66, 0.34)	12.6	11.7	11.3	1162	[42]
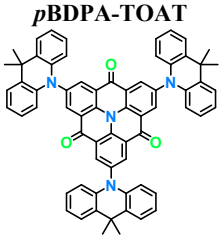 **DMAC-TOAT**	656	104/0.33	(0.59, 0.39)	2.1	1.5	1.5	945	[42]

[a] EL peak wavelength. [b] Full-width at half-maximum. [c] Commission Internationale de L'Eclairage coordinates. [d] Turn-on voltage at 1 cd m^{-2}. [e] Maximum luminance. [f] Maximum current efficiency. [g] Maximum power efficiency. [h] Maximum external quantum efficiency. [i]M. W. (Note: * denotes device with sensitizer)

Table S6. Cartesian coordinates of **RBN-ICz** at the optimized S_0 geometry.

Atom	Coordinates (Angstroms)		
	x	y	z
C	2.0507	-0.0611	0.0397

C	2.6519	-1.3514	0.1574
C	1.7634	-2.4131	0.2949
C	0.376	-2.2202	0.2618
C	-0.1843	-0.9497	0.0789
C	0.6673	0.1923	7.99E-04
C	4.2194	0.9437	-0.0371
C	4.8716	2.1606	-0.1836
C	6.2961	2.0486	-0.2205
C	6.925	0.7974	-0.1277
C	6.1814	-0.4177	0.0062
C	4.8048	-0.2733	0.0516
N	2.8607	1.0474	-0.0318
C	2.5343	2.3644	-0.1748
C	3.7494	3.1257	-0.2742
C	6.359	-1.8631	0.093
C	5.0488	-2.4701	0.1744
N	4.0803	-1.4501	0.1525
C	1.2099	2.8092	-0.2163
C	1.1149	4.2084	-0.394
C	2.2579	5.0125	-0.4965
C	3.5677	4.498	-0.4366
C	7.4889	-2.6851	0.1009
C	7.3354	-4.0659	0.1825
C	6.0574	-4.6397	0.2543
C	4.905	-3.8559	0.2515
C	-4.2286	1.6838	0.1804

C	-3.5671	2.9279	0.2084
C	-2.1692	2.9416	0.1393
C	-1.3779	1.7748	0.0506
C	-3.501	0.5038	0.1021
C	-2.092	0.5695	0.0578
N	-1.5626	-0.7244	0.0036
C	-2.6926	-3.017	-0.2522
C	-3.9389	-3.6379	-0.2924
C	-5.1539	-2.9374	-0.16
C	-5.0903	-1.5503	-0.0121
C	-3.856	-0.9009	0.0276
C	-2.6463	-1.6348	-0.0603
B	0.1517	1.6662	-0.0683
C	-4.4016	4.2139	0.307
C	-3.5281	5.479	0.3186
C	-5.3555	4.2994	-0.9042
C	-5.2283	4.1874	1.6109
C	-6.4802	-3.7084	-0.2024
C	-6.6057	-4.4424	-1.5551
C	-6.5075	-4.74	0.9462
C	-7.6956	-2.7808	-0.0441
H	2.1359	-3.4172	0.4454
H	-0.252	-3.0795	0.4318
H	6.9165	2.9321	-0.3282
H	8.009	0.7637	-0.1673
H	0.1437	4.6852	-0.4707

H	2.1313	6.0821	-0.6327
H	4.4155	5.1705	-0.5243
H	8.4784	-2.2424	0.0414
H	8.2113	-4.7064	0.1887
H	5.958	-5.719	0.3131
H	3.9315	-4.3256	0.301
H	-5.3126	1.6418	0.2209
H	-1.6555	3.8921	0.1642
H	-1.8057	-3.6115	-0.4126
H	-3.9602	-4.7123	-0.4419
H	-5.9942	-0.9579	0.0622
H	-4.1662	6.365	0.39
H	-2.8448	5.4924	1.1734
H	-2.9356	5.5702	-0.5972
H	-5.962	5.2099	-0.8492
H	-6.0385	3.4462	-0.944
H	-4.791	4.3196	-1.8415
H	-5.9054	3.3291	1.6437
H	-4.5721	4.1292	2.4848
H	-5.8352	5.0952	1.6974
H	-7.5479	-4.9992	-1.6008
H	-6.5878	-3.7302	-2.3858
H	-5.7898	-5.1543	-1.7073
H	-7.4467	-5.3036	0.9307
H	-6.4226	-4.242	1.917
H	-5.6859	-5.4571	0.8655

H	-7.674	-2.245	0.9101
H	-7.7507	-2.0439	-0.8516
H	-8.616	-3.3718	-0.0722

3. References

(1) A. D. Becke, *J. Chem. Phys.* **1993**, *98*, 5648.

(2) C. Lee, W. Yang, R. G. Parr, *Phys. Rev. B* **1988**, *37*, 785.

(3) R. Krishnan, J. S. Binkley, R. Seeger, J. Pople, *J. Chem. Phys.* **1980**, *72*, 650.

(4) S. Grimme, J. Antony, S. Ehrlich, H. Krieg, *J. Chem. Phys.* **2010**, *132*, 154104.

(5) Gaussian 09, Revision D.01, M. J. Frisch, G. W. Trucks, H. B. Schlegel, G. E. Scuseria, M. A. Robb, J. R. Cheeseman, G. Scalmani, V. Barone, B. Mennucci, G. A. Petersson, H. Nakatsuji, M. Caricato, X. Li, H. P. Hratchian, A. F. Izmaylov, J. Bloino, G. Zheng, J. L. Sonnenberg, M. Hada, M. Ehara, K. Toyota, R. Fukuda, J. Hasegawa, M. Ishida, T. Nakajima, Y. Honda, O. Kitao, H. Nakai, T. Vreven, J. A. Montgomery, Jr., J. E. Peralta, F. Ogliaro, M. Bearpark, J. J. Heyd, E. Brothers, K. N. Kudin, V. N. Staroverov, T. Keith, R. Kobayashi, J. Normand, K. Raghavachari, A. Rendell, J. C. Burant, S. S. Iyengar, J. Tomasi, M. Cossi, N. Rega, J. M. Millam, M. Klene, J. E. Knox, J. B. Cross, V. Bakken, C. Adamo, J. Jaramillo, R. Gomperts, R. E. Stratmann, O. Yazyev, A. J. Austin, R. Cammi, C. Pomelli, J. W. Ochterski, R. L. Martin, K. Morokuma, V. G. Zakrzewski, G. A. Voth, P. Salvador, J. J. Dannenberg, S. Dapprich, A. D. Daniels, O. Farkas, J. B. Foresman, J. V. Ortiz, J. Cioslowski, D. J. Fox, Gaussian, Inc., Wallingford CT, 2013.

(6) Y. Zhao, D. G. Truhlar, *Theor. Chem. Acc.* **2007**, *120*, 215.

(7) T. Lu, F. Chen, *J. Comput. Chem.* **2012**, *33*, 580.

(8) W. Humphrey, A. Dalke, K. Schulten, *J. Mol. Graph.* **1996**, *14*, 33.

(9) a) I. H. M. van Stokkum, D. S. Larsen, R. van Grondelle, BBA-Bioenergetics 2004, 1657, 82; b) K. M. Mullen, I. H. M. van Stokkum, J. Stat. Softw. 2007, 18, 1–46.

(10) X. Yan, Z. Li, Q. Wang, Y. Qu, Y. Xu, Y. Wang, *J. Mater. Chem. C* **2022**, *10*, 15408.

(11) F. Liu, Z. Cheng, L. Wan, Z. Feng, H. Liu, H. Jin, L. Gao, P. Lu, W. Yang, *Small* **2021**, *18*, 2106462.

(12) F. Huang, X. Fan, Y. Cheng, H. Wu, Y. Shi, J. Yu, K. Wang, C. Lee, X.-H. Zhang, *Mater. Horiz.* **2022**, *9*, 2226.

(13) W. Xue, H. Yan, Y. He, L. Wu, X. Zhang, Y. Wu, J. Xu, J. He, C. Yan, H. Meng, *Chem. Eur. J.* **2022**, *28*, e202201006.

(14) Y. Liu, X. Xiao, Y. Ran, Z. Bin, J. You, *Chem. Sci.* **2021**, *12*, 9408.

(15) W. Yang, J. Miao, F. Hu, Y. Zou, C. Zhong, S. Gong, C. Yang, *Adv. Funct. Mater.* **2023**, *33*, 2213056.

(16) M. Du, M. Mai, D. Zhang, L. Duan, Y. Zhang, *Chem. Sci.* **2024**, *15*, 3148.

(17) X. Cai, Y. Pan, X. Song, C. Li, Y. Pu, X. Zhuang, H. Bi, Y. Wang, *Adv. Optical Mater.* **2024**, *12*, 2302811.

(18) Y. C. Cheng, X. C. Fan, F. Huang, X. Xiong, J. Yu, K. Wang, C. S. Lee, X.-H. Zhang, *Angew. Chem. Int. Ed.* **2022**, *61*, e202212575.

(19) X. C. Fan, F. Huang, H. Wu, H. Wang, Y. C. Cheng, J. Yu, K. Wang, X.-H. Zhang, *Angew. Chem. Int. Ed.* **2023**, *62*, e202305580.

(20) K. R. Naveen, S. J. Hwang, H. Lee, J. H. Kwon, *Adv. Electron. Mater.* **2022**, *8*, 2101114.

(21) H. Chen, M. Du, C. Qu, Q. Jin, Z. Tao, R. Ji, G. Zhao, T. Zhou, Y. Lou, Y. Sun, W. Jiang, L. Duan, Y. Zhang, *Angew. Chem. Int. Ed.* **2025**, *64*, e202415400.

(22) H. Chen, T. Fan, G. Zhao, D. Zhang, G. Li, W. Jiang, L. Duan, Y. Zhang, *Angew. Chem. Int. Ed.* **2023**, *62*, e202300934.

(23) X. Cai, Y. Xu, Y. Pan, L. Li, Y. Pu, X. Zhuang, C. Li, Y. Wang, *Angew. Chem. Int. Ed.* **2023**, *62*, e202216473.

(24) M. Yang, I. S. Park, T. Yasuda, *J. Am. Chem. Soc.* **2020**, *142*, 19468.

(25) Y. Hu, M. Huang, H. Liu, J. Miao, C. Yang, *Angew. Chem. Int. Ed.* **2023**, *62*, e202312666.

(26) Y. Zou, J. Hu, M. Yu, J. Miao, Z. Xie, Y. Qiu, X. Cao, C. Yang, *Adv. Mater.* **2022**, *34*, 2201442.

(27) T. Fan, M. Du, X. Jia, L. Wang, Z. Yin, Y. Shu, Y. Zhang, J. Wei, D. Zhang, L. Duan, *Adv. Mater.* **2023**, *35*, 2301018.

(28) Y.-Y. Jing, N. Li, X. Cao, H. Wu, J. Miao, Z. Chen, M. Huang, X. Wang, Y. Hu, Y. Zou, C. Yang, *Sci. Adv.* **2023**, *9*, eadh8296.

(29) J. He, Y. Xu, S. Luo, J. Miao, X. Cao, Y. Zou, *Chem. Eng. J.* **2023**, *471*, 144565.

(30) J. Miao, G. Chen, J. He, Z. Xiao, X. Song, M. Wang, M. Huang, K. Li, X. Cao, Y. Zou, C. Yang, *Adv. Funct. Mater.* **2024**, *34*, 2316323.

(31) Y. Wang, K. Zhang, F. Chen, X. Wang, Q. Yang, S. Wang, S. Shao, L. Wang, *Chin. J. Chem.* **2022**, *40*, 2671.

(32) H. Wang, Y.-C. Cheng, X.-C. Fan, D.-Y. Chen, X. Xiong, X.-Y. Hao, Y.-Z. Shi, J. Yu, D.-X. Huang, J.-X. Chen, K. Wang, X.-H. Zhang, *Sci. Bull.* **2024**, *69*, 2983.

(33) M. Hayakawa, X. Tang, Y. Ueda, H. Eguchi, M. Kondo, S. Oda, X.-C. Fan, G. N. Iswara Lestanto, C. Adachi, T. Hatakeyama, *J. Am. Chem. Soc.* **2024**, *146*, 18331.

(34) Y. Zou, J. He, N. Li, Y. Hu, S. Luo, X. Cao, C. Yang, *Mater. Horiz.* **2023**, *10*, 3712.

(35) G. Meng, J. Zhou, X. S. Han, W. Zhao, Y. Zhang, M. Li, C. F. Chen, D. Zhang, L. Duan, *Adv. Mater.* **2024**, *36*, 2307420.

(36) Y. Zhang, D. Zhang, T. Huang, A. J. Gillett, Y. Liu, D. Hu, L. Cui, Z. Bin, G. Li, J. Wei, L. Duan, *Angew. Chem. Int. Ed.* **2021**, *60*, 20498.

(37) T. Hua, N. Li, Z. Huang, Y. Zhang, L. Wang, Z. Chen, J. Miao, X. Cao, X. Wang, C. Yang, *Angew. Chem. Int. Ed.* **2024**, *63*, e202318433.

(38) Y. Pu, X. Cai, Y. Qu, W. Cui, L. Li, C. Li, Y. Zhang, Y. Wang, *Angew. Chem. Int. Ed.* **2024**, *64*, e202420253.

(39) Y. Pu, Q. Jin, Y. Zhang, C. Li, L. Duan, Y. Wang, *Nat. Commun.* **2025**, *16*, 332.

(40) L. Ge, W. Zhang, Y.-H. Hao, M. Li, Y. Liu, M. Zhou, L.-S. Cui, *J. Am. Chem. Soc.* **2024**, *146*, 32826.

(41) Z. Yang, D. Liu, X. Cheng, T. Wang, Z. Li, G. X. Yang, Z. Chen, J. Hu, Y. Fu, X. Nie, Y. Ren, Y. Zeng, Y. Chen, K. Liu, M. Li, S. J. Su, *Angew. Chem. Int. Ed.* **2025**, *64*, e202423602.

(42) X.-C. Fan, K. Wang, Y.-Z. Shi, J.-X. Chen, F. Huang, H. Wang, Y.-N. Hu, Y. Tsuchiya, X.-M. Ou, J. Yu, C. Adachi, X.-H. Zhang, *Adv. Optical Mater.* **2022**, 10, 2101789.